

# GALICS – VI. Modelling Hierarchical Galaxy Formation in Clusters

B. Lanzoni,<sup>1\*</sup> B. Guiderdoni,<sup>2</sup> G.A. Mamon,<sup>3,4</sup> J. Devriendt,<sup>2</sup> S. Hatton<sup>3</sup>

<sup>1</sup>INAF-Osservatorio Astronomico di Bologna, Via Ranzani 1, 40125 Bologna, Italy

<sup>2</sup>Observatoire Astronomique de Lyon, 9 avenue Charles André, 69561 Saint-Genis-Laval Cedex

<sup>3</sup>Institut d'Astrophysique de Paris (CNRS UMR 7095), 98 bis Boulevard Arago, 75014 Paris, France

<sup>4</sup>GEPI(CNRS UMR 8111), Observatoire de Paris, 92195 Meudon, France

Accepted; Received; in original form

## ABSTRACT

High-resolution N-body re-simulations of 15 massive ( $10^{14} - 10^{15} M_{\odot}$ ) dark matter haloes have been combined with the hybrid galaxy formation model GalICS (Hatton et al. 2003), to study the formation and evolution of galaxies in clusters, within the framework of the hierarchical merging scenario. This paper describes the high-resolution resimulation technique used to build the dark matter halo sample, and discusses its reliability. New features incorporated in GalICS include a better description of galaxy positioning after dark matter halo merger events, a more reliable computation of the temperature of the inter-galactic medium as a function of redshift, that also takes into account the reionisation history of the Universe, and a semi-analytic description of the ram pressure stripping of cold gas from galactic discs, suffered by galaxies during their motion through the diffuse hot intra-cluster medium. Within the multitude of available model results, we choose to focus here on the luminosity functions, morphological fractions and colour distributions of galaxies in clusters and in cluster outskirts, at  $z = 0$ . No systematic dependency on cluster richness is found either for the galaxy luminosity functions, morphological mixes, or colour distributions. Moving from higher density (cluster cores), to lower density environments (cluster outskirts), we detect a progressive flattening of the luminosity functions, an increase of the fraction of spirals and a decrease of that of ellipticals and S0s, and the progressive emergence of a bluer tail in the distributions of galaxy colours, especially for spirals. As compared to cluster spirals, early-type galaxies show a flatter luminosity function, and more homogeneous and redder colours. An overall good agreement is found between our results and the observations, particularly in terms of the cluster luminosity functions and morphological mixes. However, some discrepancies are also apparent, with too faint magnitudes of the brightest cluster members, especially in the B band, and galaxy colours tendentially too red (or not blue enough) in the model, with respect to the observations. Finally, ram pressure stripping appears to affect very little our results.

**Key words:** cosmology: theory, dark matter – galaxies: haloes, formation – galaxies: clusters: general

## 1 INTRODUCTION

In the most widely accepted model for structure formation, cold dark matter (CDM) is the dominant component of the Universe. As a consequence, the first structures that form are small dark matter (DM) haloes, whose subsequent hierarchical mergers produce larger objects. Baryons are mixed in smaller proportions with the DM particles, and their evolution follows and depends on that of the DM haloes: gas cools and collapses at the centre of the halo potential wells, thus forming stars and giving rise to the observable galaxies. When haloes merge, the galaxies they contain start orbit-

ing in the new common potential well, thus mutually interacting before they merge with one another. Therefore, galaxy formation also proceeds in a hierarchical fashion, and more massive galaxies are the end products of several mergers of smaller ones. In such a picture, a galaxy cluster corresponds to a very massive DM halo, assembled by the hierarchical merger of several smaller objects, and containing a large number of galaxies that interact with the diffuse intergalactic medium and among them; field galaxies, instead, are embedded in much less massive DM haloes, that have suffered fewer merger events. Thus, galaxy properties are expected to depend, to a certain extent, on the mass and the formation history of their host DM haloes.

\* barbara.lanzoni@bo.astro.it

From an observational point of view, cluster and field galax-

ies do indeed show different properties. While spirals represent the larger fraction of the galactic population in the field, early-type galaxies prevail in clusters, and are mainly localised in the central regions (e.g., Dressler 1980; Whitmore, Gilmore & Jones 1993; Dressler et al. 1997). Spirals in clusters are found mainly in the outer regions and they show a significant deficiency in HI gas with respect to normal disks (e.g., Chamaraux, Balkowski & Gérard 1980; Giovanelli, Chincarini & Haynes 1981). Also the fraction of dwarf galaxies appears to be larger in clusters than in the field, but the exact dependence of the shape of the galaxy luminosity function on the local density of the environment is still unclear (for recent discussion, see, e.g., De Propris et al. 2003; Lin, Mohr & Stanford 2004, and references therein). It is still a matter of debate whether these differences reside in the conditions existing at the moment when galaxies formed (“nature” hypothesis), or in their subsequent evolution (“nurture” hypothesis). Certainly, dynamical processes like dynamical friction, direct mergers, and ram pressure stripping do play a role in modifying galaxy properties, and they should be more efficient in dense environments such as clusters and groups (see Mamon 1992, 2000). Major mergers are expected to destroy galaxy disks and cause spirals to transform into ellipticals. Minor mergers and rapid encounters, often collectively termed “harassment”, should heat up the disk of a galaxy, leading to the creation of a bar that fuels matter from the disk into the bulge (e.g., Moore, Lake & Katz 1998). Moreover, the ram pressure that the hot intra-cluster gas exerts on the galactic interstellar medium can lead to the removal of substantial amounts of cold gas from discs (Gunn & Gott 1972), thus contributing at modifying their morphology, star formation rates, luminosities and colours (Biermann & Shapiro, 1979; Abadi, Moore, & Bower 1999; Kenney, van Gorkom, & Vollmer 2004, and references therein).

To study galaxy evolution in clusters within the framework of the hierarchical scenario, and to try and understand how and how much it differs from that in the field, it is necessary to both follow the merging history of very massive DM haloes (the hosts of galaxy clusters), and describe the physical processes that affect galaxy properties in dense environments. The approach we have chosen employs the so-called *hybrid* technique (Roukema et al. 1997; Kauffmann et al. 1999; Diaferio et al. 2001; Springel et al. 2001b; Mathis et al. 2002; Okamoto & Nagashima 2001 and 2003; Hatton et al. 2003; Helly et al. 2003; De Lucia, Kauffmann & White 2004b), that combines N-body simulations for following the formation and merging history of DM haloes, and semi-analytical modelling for describing the physics of the baryonic component (e.g., Kauffmann, White & Guiderdoni 1993; Somerville & Primack 1999; Cole et al. 2000, and references therein).

Using N-body simulations for the DM component allows one to directly follow the highly non-linear dynamics of collapses and mergers, and thus to derive realistic and reliable halo formation and merging histories. As a drawback, the mass resolution is usually limited to unsuitably high values: typically, the particle mass in cosmological N-body simulations is some  $10^{10}M_{\odot}$ , and only haloes composed of at least 10 particles can be reliably detected. This means that a hybrid galaxy formation model applied to a typical N-body simulation allows one to resolve only galaxies more massive than few  $10^{10}M_{\odot}$  (assuming a dark-to-light mass ratio of about 10). Moreover, the smallest galaxies can only be detected, but no information about their formation history can be obtained, since they derive from the hierarchical assembly of smaller systems, not resolved in the model. To reduce this problem, high-resolution re-simulation techniques exist that allow an increase, at relatively small computational cost, of the mass resolution of a

given region (for instance, a massive DM halo) selected in a larger-scale, lower-resolution N-body simulation.

The semi-analytical modelling uses a set of simplified “recipes” for describing the processes that act on the baryonic component within the DM haloes: gas cooling, star formation, energy feedback from supernovae, galaxy interactions, etc. While the physics of these mechanisms is very complex, the use of simplified prescriptions, formulated on observationally or phenomenologically motivated basis, has the main advantage of allowing one to easily modify or switch on/off one given process, and thus to estimate its role in affecting galaxy properties. For instance, as we have done here, one can include in the model the description of ram pressure stripping of cold gas from galactic discs, and easily study how results change when this process is taken into account or not.

In the present paper, we study galaxy formation and evolution in clusters by re-simulating at high resolution a sample of 15 massive DM haloes, and by using a semi-analytical model to follow the evolution of the baryonic component. In Section 2, we describe our cluster-size DM haloes sample and the resimulation technique we have employed to obtain it. The package we use to analyse these N-body simulations and to describe the physical and spectro-photometric evolution of galaxies within the haloes is called GalICS (for *Galaxies In Cosmological Simulations*). It is described in detail and tested against several observations of the local Universe in the first paper of this series (Hatton et al. 2003), and it has been used to reproduce and predict many properties of the Lyman Break Galaxies at  $z \simeq 3$  in Blaizot et al. (2004). Here, we apply it to the cluster environment, after introducing slight modifications required by the improved mass resolution, and taking into account the ram pressure stripping process. Its main characteristics and the new physical processes we have introduced in the model are summarised in Section 3. The results we find in terms of the galaxy luminosity functions, morphological fractions and colour distributions are presented in Section 4. The analysis mainly aims at studying if and how these properties vary with cluster richness, and with the local density of the environment. Discussions and conclusions are presented in Section 5.

In order to facilitate the comparison to model results, observations presented here have been rescaled using  $H_0 = 70 \text{ km s}^{-1} \text{ Mpc}^{-1}$ .

## 2 THE CLUSTER-SIZE DM HALO SAMPLE

### 2.1 Parent simulation

Under our working hypothesis, a cluster of galaxies is hosted by a very massive ( $10^{14}$ – $10^{15}M_{\odot}$ ) DM halo. With the aim of studying galaxy formation in clusters with some statistical significance, a sample of 15 DM haloes in this mass range has been selected from the dissipationless “Very Large Simulations” (VLS; see Yoshida, Sheth, & Diaferio 2001), where the comoving volume of the Universe is sufficiently large to contain several high-mass objects: the box size is  $479 \text{ Mpc}/h$ , with  $H_0 = 100 h^{-1} \text{ km s}^{-1} \text{ Mpc}^{-1}$ , and  $h = 0.7$ . The adopted cosmological model is the “standard”  $\Lambda$ CDM, with  $\Omega_m = 0.3$ ,  $\Omega_{\Lambda} = 0.7$ , spectral shape  $\Gamma = 0.21$ , and normalisation to the cluster local abundance,  $\sigma_8 = 0.9$ . The total number of particles is  $512^3$ , of  $6.86 \cdot 10^{10}M_{\odot}/h$  mass each.

DM haloes have been detected in these simulations by means of the spherical overdensity criterion (Lacey & Cole 1994; Tormen, Bouchet & White 1997), i.e., they are defined as spheres centred on maximum density peaks in the particle distribution, with mean density  $\rho_{\Delta}$  as predicted by the spherical top-hat model: for the adopted

$\Lambda$ CDM cosmology,  $\rho_{\Delta} \simeq 97 \rho_{\text{crit}}$  at  $z = 0$  (Eke, Cole & Frenk 1996), with  $\rho_{\text{crit}}$  being the critical density of the Universe at that redshift. The radius  $r_{\Delta}$  of such spheres thus defines the boundary of DM haloes, to be distinguished from the *virial* radius  $r_{\text{vir}}$ , that we estimate from the measured potential and kinetic energies. Among all, we have selected a sample of 15 haloes with total masses  $M_{\Delta}$  ranging between  $10^{14}$  and  $2.3 \cdot 10^{15} M_{\odot}/h$  (see second and third columns of Table 1 for the values of  $M_{\Delta}$  and  $r_{\Delta}$  in our sample). They span a variety of shapes, from nearly round to more elongated. The richness of their environment also changes from case to case, with the less isolated haloes usually surrounded by pronounced filamentary structures, containing massive (up to 20% of the selected halo mass) neighbours.

Given the particle mass of the VLS, only haloes of at least  $\sim 7 \cdot 10^{11} M_{\odot}$  (10 particles) can be detected, and no information about the formation history of the smallest can be obtained. This clearly limits the reliability of any galaxy formation model based on such simulations, since all galaxies fainter than about  $L_{*}$ , which are an important fraction of the overall galactic population and the building blocks of brighter galaxies, cannot be resolved. For that reason, we have re-simulated the 15 haloes of our sample and increased their mass resolution by a factor  $\sim 33$  or more, as described below (see also Lanzoni, Cappi & Ciotti 2003; Lanzoni et al. 2004; De Lucia et al. 2004a and 2004b).

## 2.2 High-resolution re-simulations

The technique we use (Tormen et al. 1997) consists in selecting a halo in a given cosmological simulation, and “zooming in” on it. The first step is to draw a spherical region around the selected halo in the parent simulation. The radius of such a region ( $r_{\text{dec}}$ ) is of few  $r_{\Delta}$ , so that it contains all the particles composing the halo, plus those in a boundary layer around it. The number of particles contained within this region (that is called the *high resolution region*) in the initial conditions of the simulation is then increased, until the desired mass resolution is achieved. As a consequence, the mean inter-particle separation decreases, and it becomes necessary to add the corresponding high-frequency modes of the fluctuation spectrum to the waves on larger scales used in the initial set up of the parent simulation. The displacement field corresponding to these high-frequency modes is also computed and added to that of the original parent simulation. The distribution of particles surrounding the central high resolution (HR) region is smoothed by means of a spherical grid, whose spacing increases with the distance from the centre: in such a way, the original surrounding particles are replaced by a smaller number of *macro-particles*, whose mass grows with the distance from the HR region. Thanks to this method, the total number of particles to be evolved in the simulation remains small enough to require reasonable computational resources. At the same time, the tidal field that the overall particle distribution exerts on the HR region is kept very close to the original one, and the boundary layer of HR particles around the selected halo prevents its “contamination” by lower-resolution macro-particles during the simulation. This implies that the boundary layer has to become larger when the mass of the selected halo decreases, and/or the local density around it increases, and/or the mass resolution one wants to attain increases. The resulting particle distribution in the new initial conditions is spherical, with a diameter equal to the box size of the parent simulation, and with vacuum boundary conditions (i.e., a vanishing density fluctuation field outside the sphere). An N-body simulation is then run starting from these new initial

conditions, and the properties of the selected halo are recomputed at the desired higher resolution.

We have applied such a technique to the 15 massive DM haloes selected in the VLS. To run the resimulations, we have used the parallel dissipationless tree-code GADGET (Springel, Yoshida & White 2001a), on the IBM SP2 of the CINES (Montpellier, France), and the CRAY T3E of the RZG Computing Center (Munich, Germany). The resolution in mass has been increased by a factor  $\sim 33$  for the 5 most and the 5 least massive haloes, using high-resolution particles of  $\sim 2 \cdot 10^9 M_{\odot}/h$  each, while a further factor of 2 in mass resolution was achieved for the 5 intermediate mass haloes (leading to a particle mass of  $10^9 M_{\odot}/h$  in this case). As a consequence, dark matter haloes with masses down to 2 and  $1 \times 10^{10} M_{\odot}/h$  can now be resolved in our resimulations. The Plummer equivalent gravitational softening used for the HR region is  $\epsilon = 5 \text{ kpc}/h$ , corresponding to about 0.2% and 0.5% of the radius  $r_{\Delta}$  for the most and the least massive haloes, respectively. This scale length, which is a fair estimate of our spatial resolution, is to be compared with that of  $30 \text{ kpc}/h$  in the original VLS. To prevent low-resolution macro-particles to end within the final resimulated halo, a radius  $r_{\text{dec}}$  of about 3 to  $5 r_{\Delta}$  was necessary for the most, and the least massive haloes. The resulting number of high and low resolution particles used for the resimulation runs are listed in Table 1 (columns 4 and 5); note that to get the same mass resolution in the entire volume of the parent simulation, about  $1650^3$  particles would have been required. Results have been dumped in files for 100 temporal outputs, logarithmically spaced in the expansion factor of the Universe between  $z = 20$  and  $z = 0$ , yielding a time resolution of about 400 Myr in the worst case, i.e., around  $z = 0$ .

Images of the 15 haloes after resimulations are shown in Figure 1. Their masses and radii are listed in columns 6 and 7 of Table 1. They differ by a few percent from the original values (columns 2 and 3 of the same table), because the overall gravitational field in the resimulations is not exactly identical to the original one in the VLS. These differences are smaller than 10% in mass and 4% in radius for the 10 most massive haloes, while they are slightly larger for the lighter objects. Halo g914 represents an extreme case: its high-resolution mass and radius are respectively 45% and 13% larger than its low resolution values. This can be explained by noticing that, in the parent simulation, g914 had a neighbouring halo with a mass of  $\sim 2 \cdot 10^{13} M_{\odot}/h$  (equal to 20% of its mass), at a distance of about  $2.5 r_{\Delta}$ . This object is not found anymore in the resimulation, where, instead, two haloes of  $1.5$  and  $4.5 \cdot 10^{12} M_{\odot}/h$  are found at  $3 r_{\Delta}$ , and another one of  $1.5 \cdot 10^{13} M_{\odot}/h$  is at a distance of  $3.5 r_{\Delta}$ . It is therefore possible that, due to the lack of a massive neighbour in the resimulation, g914 has been able to accrete more matter, resulting in a mass and radius increase by an important fraction.

In summary, we can assess that the high-resolution re-simulation technique is reliable, in the sense that it reproduces quite accurately the selected halo properties (and those of a number of other objects within the boundary layer around them) at increased mass resolution (see also Gao et al. 2004). Thanks to our 15 resimulations, we are therefore able to describe galaxy formation and evolution in clusters and in their outskirts in much more detail than we would if we were using the VLS alone.

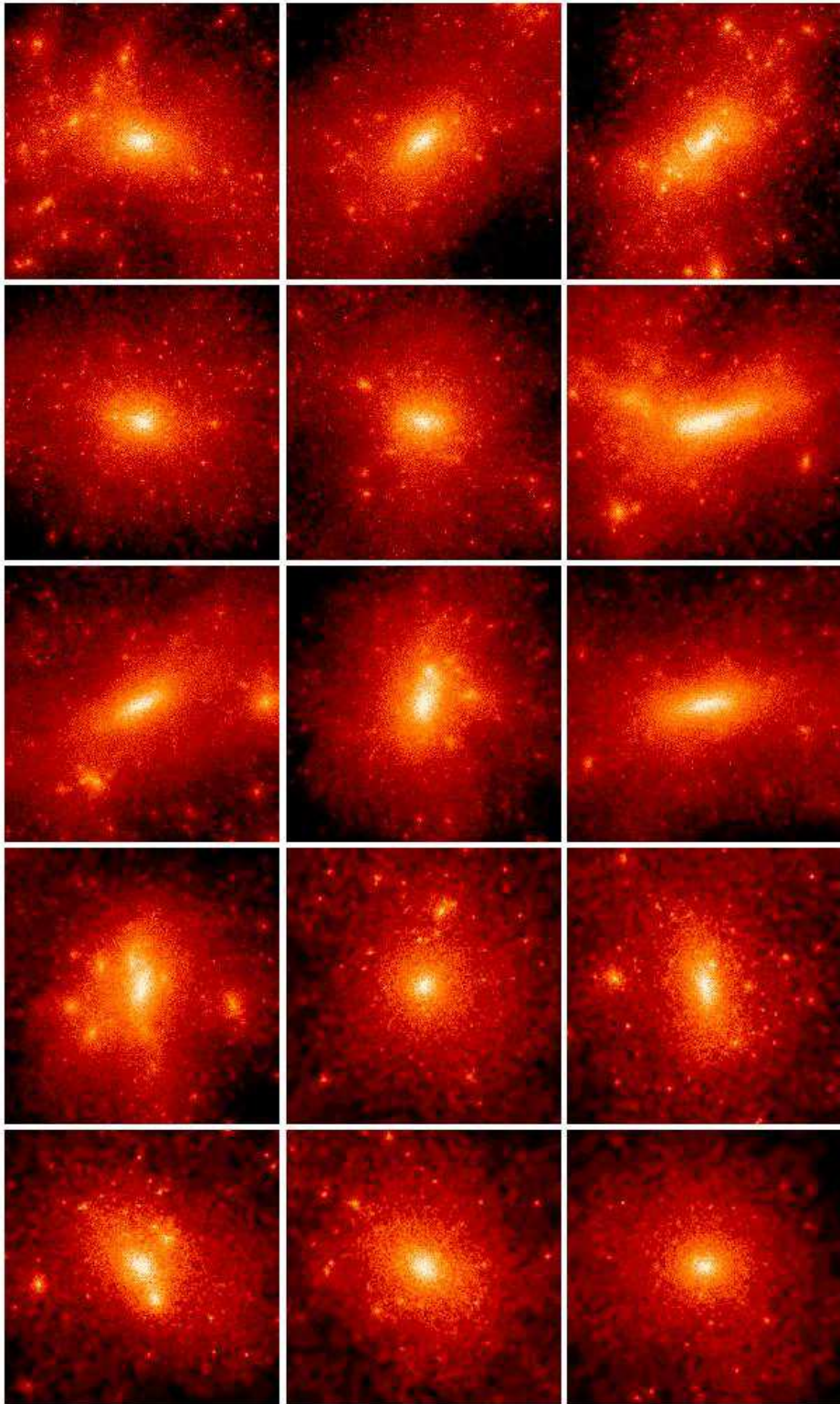


**Figure 1.** Images of the 15 DM haloes in the high-resolution resimulations at  $z = 0$ . Panels show the projection along the  $z$ -axis of a cubic region of about  $2r_\Delta$  side centred on each halo. Particle density increases from black to white. Haloes are ordered from left to right, then top to bottom as listed in Table 1 (decreasing order of mass in the low-resolution simulations).

**Table 1.** Characteristics of the 15 DM haloes in our sample. *Columns 2 and 3:* masses (in  $M_{\odot}/h$ ) and radii (in  $\text{Mpc}/h$ ) of the 15 DM haloes in the parent VLS simulations, as measured by the spherical overdensity halo finder ( $\Delta \simeq 97$  at  $z = 0$  for the adopted cosmology); *columns 4 and 5:* numbers of high-resolution and low-resolution particles used in the resimulation runs; *columns 6 and 7:* halo masses and radii after resimulations; *columns 8 and 9:* number of galaxies brighter than  $M_B = -17$  and  $-19$ , respectively, found within the halo virial radius  $r_{\text{vir}}$ .

Name	$M_{\Delta}$	$r_{\Delta}$	$n_{\text{HR}}$	$n_{\text{LR}}$	$M_{\Delta}$	$r_{\Delta}$	$N_{17}$	$N_{19}$
g8	$2.29 \cdot 10^{15}$	2.72	3700120	191733	$2.34 \cdot 10^{15}$	2.75	1642	374
g1	$1.39 \cdot 10^{15}$	2.30	2574717	202301	$1.40 \cdot 10^{15}$	2.31	1139	263
g696	$1.30 \cdot 10^{15}$	2.26	4870197	184314	$1.14 \cdot 10^{15}$	2.16	901	235
g51	$1.20 \cdot 10^{15}$	2.20	1677364	213477	$1.08 \cdot 10^{15}$	2.12	884	191
g72	$1.16 \cdot 10^{15}$	2.17	3299865	194277	$1.18 \cdot 10^{15}$	2.18	908	229
g245	$7.08 \cdot 10^{14}$	1.84	3437317	215269	$6.50 \cdot 10^{14}$	1.79	487	103
g689	$5.95 \cdot 10^{14}$	1.74	3252085	215809	$6.08 \cdot 10^{14}$	1.75	613	126
g564	$4.98 \cdot 10^{14}$	1.64	2068981	227187	$4.91 \cdot 10^{14}$	1.63	433	94
g1777	$4.02 \cdot 10^{14}$	1.52	3094123	219047	$3.83 \cdot 10^{14}$	1.50	342	64
g4478	$2.99 \cdot 10^{14}$	1.38	2293433	225706	$2.92 \cdot 10^{14}$	1.37	205	41
g6212	$1.01 \cdot 10^{14}$	0.95	271228	246780	$1.12 \cdot 10^{14}$	1.00	92	23
g3344	$1.01 \cdot 10^{14}$	0.96	206140	248756	$1.09 \cdot 10^{14}$	0.99	84	24
g914	$1.00 \cdot 10^{14}$	0.96	250605	247091	$1.45 \cdot 10^{14}$	1.09	52	10
g676	$1.00 \cdot 10^{14}$	0.96	210958	248817	$1.05 \cdot 10^{14}$	0.98	94	17
g1542	$1.00 \cdot 10^{14}$	0.96	207202	248948	$8.22 \cdot 10^{13}$	0.99	78	15

### 3 THE GALICS GALAXY FORMATION MODEL

#### 3.1 General overview

Once the N-body simulations for the DM component have been run, we have used the GalICS hybrid galaxy formation model to study galaxy formation and evolution within the haloes. The model consists in three main steps: 1) detecting DM haloes in the outputs of the N-body simulation; 2) constructing their merging history trees; 3) describing the physics of the baryonic component within the haloes by means of a semi-analytical technique (e.g., White & Frenk 1991; Kauffmann et al. 1993; Cole et al. 1994; Somerville & Primack 1999). Its main features are described below, but we refer to Hatton et al. (2003) for full details.

To identify DM haloes in the outputs of our high resolution resimulations, we use a *friends-of-friends* algorithm (Davis et al. 1985), with linking-length parameter  $b = 0.2$ , in units of the mean inter-particle separation. Only haloes with at least 10 particles (i.e.,  $\sim 1-2 \times 10^{10} M_{\odot}/h$ ) are detected, since smaller groups are usually dynamically unstable (Kauffmann et al. 1999).

Haloes of each timestep are then linked to those in the preceding and in the successive outputs, by following the DM particles they have in common. A sort of genealogical tree is therefore built, where parents and descendants are recorded. Events of diffuse matter accretion and halo fragmentation can also take place and contribute to increase/decrease the mass of the resulting halo.

Galaxy properties are then computed and evolved through the DM halo merging tree, by means of simplified “recipes”, physically or phenomenologically motivated, that are able to describe the processes acting on gas and stars. The overall scheme of our semi-analytical model is similar to that of others:

- gas cools and forms stars in an exponential, rotationally supported disc at the centre of newly detected DM haloes, provided that they are bound and that their spin parameter  $\lambda < 0.5$ ;
- supernovae explosions reheat the gas and possibly eject it out

from the disc or the halo, thus inhibiting future star formation, and spreading metals into the interstellar medium;

- when haloes merge, the galaxies they contain start orbiting in one common potential well, and dynamical interactions take place: orbital decay, due to dynamical friction against the background DM particles, makes galaxies sink towards the centre of the halo where they eventually merge with the central galaxy; direct mergers can also take place between satellite (non central) galaxies.

Within this scheme, morphological transformations from discs to spheroids are driven by merger events, with an efficiency that depends on the initial mass ratio of the interacting galaxies. Note that disc instabilities are also taken into account as possible mechanisms for feeding central spheroidal components. New discs of cold star-forming gas can be later accreted by the spheroids, and spiral galaxies, with a more or less prominent bulge, thus form. Stellar spectra are computed along the full merging history of galaxies by means of a spectrophotometric model, so that galaxy luminosities and colours are obtained at every timestep. For this purpose, we use STARDUST (Devriendt, Guiderdoni & Sadat 1999), which also takes into account the effects of dust absorption and emission.

As in GALICS I, galaxies are morphologically classified by their bulge-to-disc luminosity ratio in the B band. Following Simien & de Vaucouleurs (1986), we define a morphological index  $I \equiv \exp(-L_B/L_D)$ , so that  $I = 1$  for a pure disc,  $I = 0$  for a pure bulge, and the different morphological types correspond to the following intervals of it:  $I \leq 0.219$  for elliptical galaxies (corresponding to a bulge blue light fraction, with respect to the total,  $> 60\%$ );  $0.219 < I < 0.507$  for lenticulars (bulge fraction between 40% and 60%);  $I \geq 0.507$  for spirals (bulge fraction smaller than 40%). The values adopted for the free parameters are also the same as those used in GALICS I (see their Table 2).

### 3.2 New elements in the GalICS model

With respect to the original version of the model as presented in GALICS I, several modifications have been introduced in the present work.

The first change concerns galaxy positioning: by using equation (5.1) of GALICS I to place galaxies within the new common potential well after DM halo merger events, we noticed that many of our most massive clusters did not have any central galaxy, at odds with observations. We have therefore slightly modified that prescription by weighting the original ‘jumping’ distance  $R_j$  of GALICS I by the mass contribution of the progenitor halo to its son:  $R_{j,\text{new}} = R_j (1 - M_{\text{prog}}/M_{\text{son}})$ . In this way, if the progenitor contributes to most of the mass of the son, its position (and that of its central galaxy) remains practically unperturbed by the merger event, while if it is negligible, the new position of its central galaxy is determined as in GALICS I. It has been shown (Springel et al. 2001b) that correctly following the spatial distribution of galaxies within DM haloes, and thus also their merging rate, is quite important for getting the right galaxy properties, like the bright-end of the luminosity function, or the morphology-clustercentric relation. Whereas a substantial improvement in this direction will be implemented in the next version of GalICS, the method we adopt here is still simplistic and approximate, and we therefore do not attempt to reproduce in detail those observations that strongly depend on galaxy radial positions within the clusters.

Second, given the improved mass resolution of our resimulations with respect to GALICS I (thus, also a large number of low mass haloes that were not resolved there), a more accurate description of the reionisation history of the Universe is necessary to avoid an unobserved excess of galaxies at the faint-end of the luminosity function (see thin solid lines in Figure 3). For that purpose, here we compute the temperature of the inter-galactic medium as a function of redshift following Valageas & Silk (1999), and we use it as a threshold to determine whether the gas can cool and form galaxies within DM haloes. More specifically, we require that the temperature of the infalling gas (taking into account adiabatic heating as it falls in the DM potential well) be smaller than the virial temperature of the DM halo if the gas is to cool and form a central galaxy (e.g., Blanchard, Valls-Gabaud & Mamon 1992).

Finally, we include in this work the description of ram pressure stripping of cold gas from galactic discs, as they orbit through the hot intra-cluster medium. This process is thought to be responsible for the neutral hydrogen deficiency observed in cluster spirals with respect to those in the field (Gunn & Gott 1972), and has also been considered as a possible mechanism to turn disc galaxies into lenticulars (e.g., Melnick & Sargent 1977; Solanes & Salvador-Solé 1992). Despite its potential importance, such a process has only been implemented once in a hybrid model for galaxy formation (Okamoto & Nagashima 2003). This previous implementation led to the conclusion that ram pressure stripping produces negligible changes in galaxy colours, star formation rates and morphological fractions within the cluster core. These results, however, were obtained only for bright galaxies ( $L > L_*$ ) in one single cluster, while the present work allows us to extend the investigation to fainter galaxies and a larger number of clusters of different masses.

We have modelled gas stripping from discs following the original idea of Gunn & Gott (1972), who use a simple argument of equilibrium between static forces to estimate its efficiency: if the dynamical pressure due to the intra-cluster medium is larger than the gravitational force per unit surface of the disc, all cold gas be-

yond a given radius  $R_{\text{str}}$  on the disc is stripped out. For an exponential density profile, such a radius is given by:

$$\frac{R_{\text{str}}}{R_{\text{D}}} = -\ln \sqrt{\frac{\rho_{\text{ICM}}(r) v_{\perp}^2}{2\pi G \Sigma_{0\star\text{g}} \Sigma_{0\text{g}}}}, \quad (1)$$

where  $R_{\text{D}}$  is the characteristic radius of the gas and of the gas-plus-stars exponential distributions in the disc, with central surface brightness  $\Sigma_{0\text{g}}$  and  $\Sigma_{0\star\text{g}}$ , respectively;  $\rho_{\text{ICM}}(r)$  is the intra-cluster medium density at the orbital position  $r$  of the galaxy within the cluster at the beginning of each time-step;  $v_{\perp}$  is the component of the galaxy velocity perpendicular to the disc. Further assuming that the distribution of galaxy orbital velocities is a Maxwellian, with a rms velocity equal to the halo velocity dispersion (i.e.,  $\sigma = V_c/\sqrt{2}$ , for a singular isothermal sphere of circular velocity  $V_c$ ), one can randomly select the module of  $v_{\perp}$ . One then multiplies it by the sine of the angle between the velocity vector and the disc plane, this time randomly selected from a uniform distribution between 0 and 1, to finally determine  $R_{\text{str}}$ . The mass of cold gas beyond this stripping radius is then removed from the disc and added to the hot intra-cluster medium.

### 3.3 Practical considerations

We have applied the (slightly modified) GalICS model to the 15 high-resolution resimulations of massive haloes presented above. Since the halo masses span one order of magnitude, from  $10^{14}$  to  $10^{15} M_{\odot}/h$ , we have studied the dependence of galaxy properties on cluster richness (mass). Moreover, not only the main clusters, but also their outskirts were available at high resolution in every simulation; therefore, we also investigated the dependence of galaxy properties on the local environment. In particular, we distinguish among the “*whole cluster*”, i.e., the entire DM halo and its baryonic content within a sphere of radius  $r_{\text{vir}}$ ; the “*cluster core*”, i.e., DM and baryons contained within a sphere of radius  $r_{\text{vir}}/3$ ; the “*cluster envelope*”, i.e., the region between  $r_{\text{vir}}/2$  and  $r_{\text{vir}}$ ; and the “*cluster outskirts*”, i.e., all high-resolution DM haloes less massive than  $10^{14} M_{\odot}/h$  around the main cluster (within the high-resolution boundary layer), and their baryonic content. Note however that, our definitions of cluster “core” and “envelope” do not exactly match the observed ones, since they refer to 3-dimensional volumes, while observations always deal with projections along the line of sight.

Random realisations are used in some part of the semi-analytical code to determine various galaxy properties. Besides those used for the ram pressure stripping (see previous section), we use random numbers also for assigning galaxy positions within the new common potential well after DM halo mergers, and for selecting the satellite galaxies involved in direct collisions. To check how much results are sensitive to random realisations, we have run the model 10 times on the same simulation, only changing the value of random seeds. We find that results are in general very robust, with a small dispersion about the mean values.

As discussed in GALICS I, the existence of a cut-off mass for the DM haloes (10 particles, in our case) introduces an effective resolution limit on our results. We therefore take as “completeness limit” for the baryonic mass of our galaxy sample the smallest halo mass times the baryonic fraction of the Universe, i.e., the galactic mass  $m_{\text{lim}} = 2 \cdot 10^{10} \times \Omega_b/\Omega_m \simeq 4 \cdot 10^9 M_{\odot}$ , where the value  $\Omega_b = 0.02/h^2$  is assumed (Tytler, Fan & Burles 1996). The tight correlation that is found between galaxy baryonic mass and magnitudes, gives in turn the following magnitude limits in the B, V,

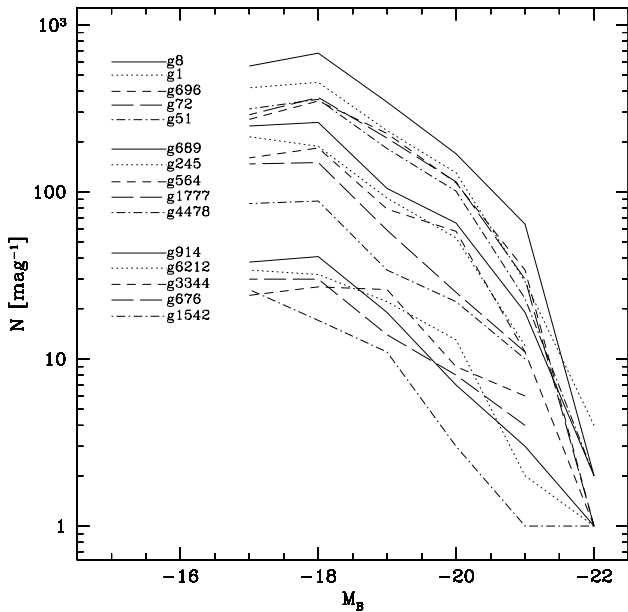


**Figure 2.** Dependence of the galaxy luminosity function on cluster mass. The B band LFs of our 15 simulated clusters are plotted in units of number of galaxies per magnitude bin. Curves are labelled with halo names, the halo mass approximately increasing along the y-axis (compare to Table 1).

and K bands:  $M_B \simeq -16.75$ ,  $M_V \simeq -17.5$ , and  $M_K \simeq -20.75$ . Galaxies fainter than these limiting magnitudes are never considered in the following.

## 4 RESULTS

### 4.1 Luminosity functions

The individual B band galaxy luminosity functions (LFs) of the 15 simulated clusters are plotted in Figure 2. The shape of the LF appears to vary from cluster to cluster (which is reminiscent of, e.g., the observations of Yagi et al. 2002), but no systematic trend is detected as the halo masses change.

The self-similarity of the cluster LF is even clearer when normalising to the number of galaxies brighter than a given magnitude, as in Figure 3 (upper panels), for  $M_B \leq -18.5$  and for  $M_K \leq -23$ : the 15 dotted lines are quite closely superimposed, and minor deviations from the average LF are independent of cluster mass. Also the LFs of the most massive cluster in GALICS I ( $3.9 \cdot 10^{14} M_\odot/h$ ) is well superimposed on those of the present 15 clusters, both in B and in K, above the completeness limits of that work (marked with arrows in the figure). We therefore conclude that, *at least in the considered cluster mass range* ( $10^{14} \div 10^{15} M_\odot$ ), *and for*  $M_B \lesssim -17$  *and*  $M_K \lesssim -21$ , *the galaxy luminosity function in clusters is universal.* This is also the conclusion of several observational studies in different photometric bands (e.g., Trentham 1998; Trentham & Mobasher 1998; Paolillo et al. 2001; De Propris et al. 2003), even if a general consensus still lacks (see, e.g., Lopez-Cruz et al. 1997; Lumsden et al. 1992; Valotto et al. 1997; Trentham & Hodgkin 2002; Lin et al. 2004). In particular, Trentham & Hodgkin (2002) detect a steepening of the faint-end of the LF for increasing cluster richness, but this trend is clear only at magnitudes fainter than  $M_B = -17$ , where our simulations start to

become incomplete. In the K band, a (mild) steepening of the faint-end LF for decreasing cluster richness, is found both by Lin et al. (2004) and in our model, but the statistical significance is poor. A more robust difference between rich and poor clusters seems to be the observed fainter luminosity of the brightest galaxies in lower mass clusters, compared to the most massive ones (De Propris et al. 2003; Lin et al. 2004), a trend that we also find in our model.

Given its apparent universality, we can compare our results to the observed *composite* LFs, obtained by combining together clusters of different richness. Figure 3 (panel a) shows that a remarkable agreement is found between the model B band LF and that obtained from 60 clusters in the 2dF Galaxy Redshift Survey (De Propris et al. 2003), which very well follows, in turn, the one derived by Trentham (1998) for 9 clusters of different richness at  $z < 0.2$ . Also in K (panel b), model results agree well with the composite LF of Trentham & Mobasher (1998) derived for 5 X-ray luminous clusters at different redshifts, that of Balogh et al. (2001) from the 2MASS and LCRS surveys, and that of Lin et al. (2004) obtained for clusters and groups from the 2MASS survey. Actually, in both bands a discrepancy is also apparent: galaxies brighter than  $M_B \simeq -22$  and  $M_K \simeq -26$  are absent in the model, but are found in the observations. Note, however, that these very bright objects are also the rarest, and we might miss them because of insufficient statistics.

The model LFs in cluster outskirts are shown in the lower panels of Figure 3. The LFs of GALICS I for the average field, both in B and in K bands, are in rather good agreement with those of our cluster outskirts, except at the faint-end, where the effects of the lower mass resolution of GALICS I rapidly become apparent. With respect to the observations (Marinoni et al. 1999 and Norberg et al. 2002, for the B band; Cole et al. 2001, in K), the overall agreement is less satisfactory than for clusters. Also in this case, the brightest observed galaxies are missed in our simulations. However, they are found in GALICS I, where the model is run on a scale supposedly representative of the “average field” of the Universe. This suggests that such a discrepancy is not a drawback of the model itself, but it is due to the fact that we are not comparing exactly the same kinds of environment here, since only the immediate outskirts of clusters, not the average field, are available in our resimulations. This same reason might also account, at least in part, for the too bright characteristic magnitude  $M_*$  of our LFs, with respect to the observations: since  $M_*$  is typically fainter in clusters, than in the field (see below), and since observational samples of the field also include data from galaxies residing in clusters, a fainter  $M_*$  for the field, than for the immediate cluster outskirts, has to be expected. In addition, as apparent from panel c, the entity of such a disagreement also depends on the data sample we compare with, since inconsistencies are still present among different observational works (for example, those between Marinoni et al. 1999 and Norberg et al. 2002, which cannot be solely attributable to uncertain transformations between their photometric systems. See, e.g., Liske et al. 2003 for an extensive discussion of disagreements among different LFs).

For a more quantitative comparison, we have fitted our LFs with the Schechter (1976) function. For magnitudes above the completeness limits, binned by half-magnitude, the Schechter parameters obtained by minimising the  $\chi^2$  of the joint fits to the 15 cluster LFs are given in Table 2, where we also list those derived by some observational works. Within the uncertainties, the Schechter parameters of the model and the observed cluster LFs agree well. Instead, with respect to the B band observations in the field,  $M_*$  is 0.13–0.78 mag too bright (depending on the observational sample of comparison), and the slope is too flat in our simulations. The

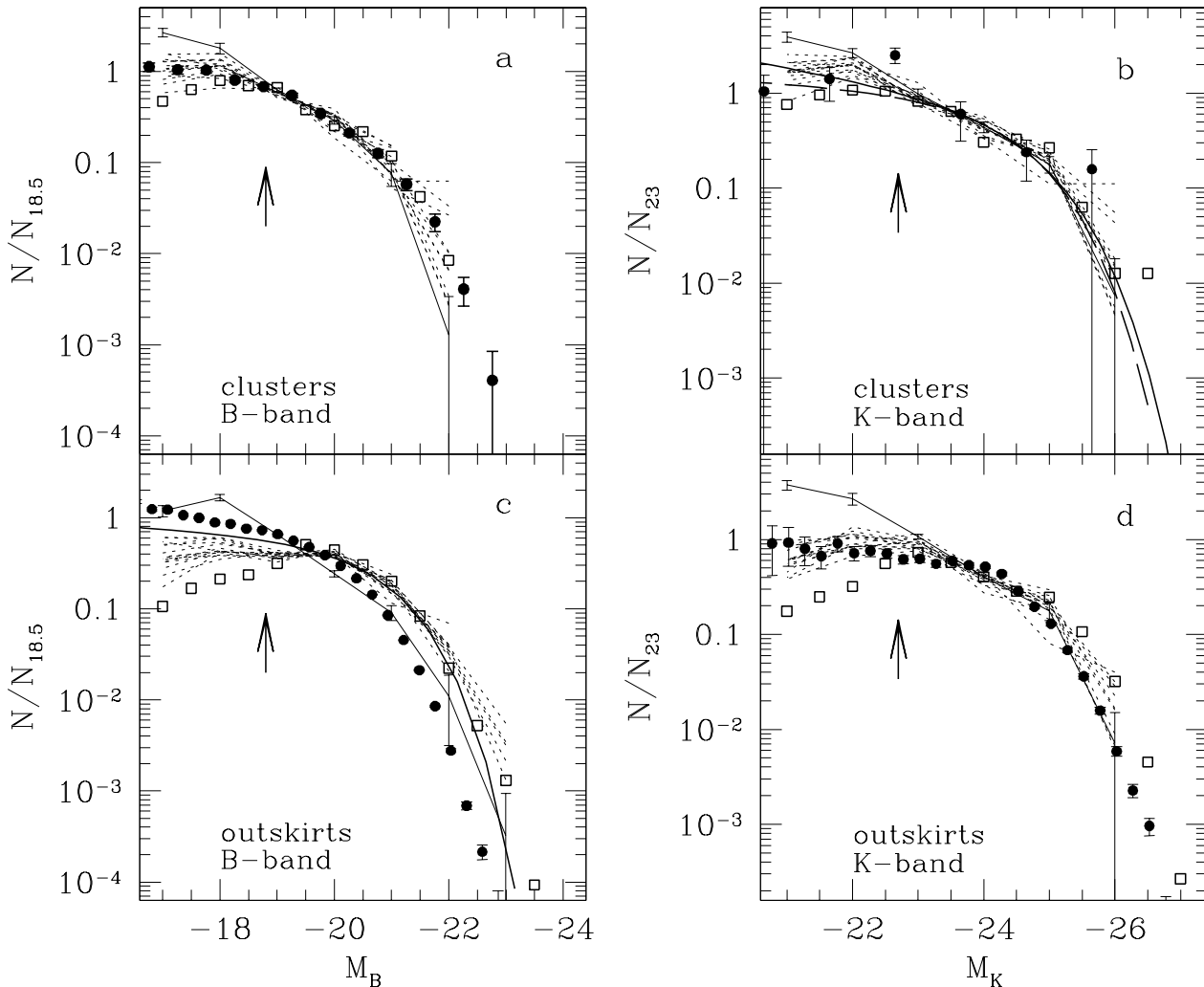


**Figure 3.** Comparison of the model LF to observations, for galaxies in clusters and in cluster outskirts, in the B and K bands. All LFs are normalised to the number of galaxies brighter than  $M_B = -18.5$  or  $M_K = -23$ . In all panels, dotted lines show the model LFs for each individual cluster. Thin solid lines mark the average LF of the 15 clusters when the reionisation history of the Universe is not taken into account. Empty squares trace the LF determined from GALICS 1 (error bars are omitted for sake of clarity), for the galaxies populating the most massive DM halo (*panels a and b*), and the average field (*panels c and d*); the magnitude resolution limits of GALICS 1 are marked with the arrows. *Panel a*: B band LFs of cluster galaxies. Solid circles represent the composite B-band LF of 60 clusters from the 2dFGRS (De Propris et al. 2003; the conversion from  $b_j$  to Johnson B is done as described in Table 2). *Panel b*: K band LFs of cluster galaxies. Solid circles represent the composite LF of 5 X-ray luminous clusters at various redshifts, as determined by Trentham & Mobasher (1998). The dashed and the solid lines are, respectively, the Schechter best-fits to the composite K band LF of clusters and groups from the 2MASS Survey by Lin et al. (2004), and from the 2MASS and LCRS surveys, as determined by Balogh et al. (2001). *Panel c*: B band LF of galaxies in cluster outskirts and in the field. Solid circles represent the field LF from 2dFGRS (Norberg et al. 2002), after the conversion from  $b_j$  to Johnson B magnitudes. The solid line trace the B band LF of Marinoni et al. (1999). *Panel d*: K band LF of galaxies in cluster outskirts and in the field. Solid circles represent the field LF from the 2dFGRS (Cole et al. 2001). See Table 2 for the values of the best-fit Schechter parameters.

“correct” slope is found with respect to the observed field LF in K, but an excess of 0.2 mag in  $M_*$  is also apparent. In any case, it is worth noticing that the values of the best fit parameters are quite dependent on several factors, like whether the brightest cluster members are included (as in our case) or not in the analysis (e.g., Lin et al. 2004), and the considered range of magnitudes (for instance, if we restrict the fits to galaxies 0.5 mag brighter than the limiting magnitudes, we find steeper faint-end slopes). Moreover, a single Schechter function often provides a poor fit to the observed LFs

(e.g., Popesso, Boehringer & Voges 2004, and references therein), and no firm agreement is yet found among different observational studies.

The dependence of the LF on environment is further studied in Figure 4, which reveals a *gradual flattening of the faint-end, when moving from denser (cluster cores), to less dense regions (cluster outskirts), a trend that we find both in K and in B bands*. Observationally, a steeper faint-end slope of the LF in clusters, and particularly in cluster cores, with respect to the field, is reported by

**Table 2.** Values of the best-fit Schechter parameters and their  $1\sigma$  error bars for the model and the observed LFs, in B and K bands. The upper part of the table refers to cluster environment, the lower part to the cluster outskirts for the model, and to the “average field” of the Universe for the observations.

Band	envmt	input	ref.	$M_*$	$\alpha$
B	cluster	simulations	G6	$-20.56^{+0.04}_{-0.10}$	$-1.34^{+0.01}_{-0.03}$
K	cluster	simulations	G6	$-24.75^{+0.07}_{-0.04}$	$-1.39^{+0.01}_{-0.01}$
B	cluster	APM+2dFGRS	DP03	$-20.58 \pm 0.07$	$-1.28 \pm 0.03$
K	cluster	2MASS+LCRS	B01	$-24.58 \pm 0.40$	$-1.30 \pm 0.43$
K	cluster	2MASS+2dFGRS	L04	$-24.34 \pm 0.01$	$-1.1$
B	outskirts	simulations	G6	$-20.95^{+0.01}_{-0.05}$	$-0.98^{+0.01}_{-0.01}$
K	outskirts	simulations	G6	$-24.41^{+0.02}_{-0.07}$	$-0.98^{+0.02}_{-0.02}$
B	field	NOG	M99	$-20.82 \pm 0.08$	$-1.1 \pm 0.06$
B	field	APM+2dFGRS	N02	$-20.17 \pm 0.07$	$-1.21 \pm 0.03$
K	field	2MASS+2dFGRS	Co01	$-24.21 \pm 0.03$	$-0.96 \pm 0.05$

Notes: envmt = environment; refs. = references: G6 = GALICS VI (this paper); DP03 = De Propris et al. (2003); B01 = Balogh et al. (2001); L04 = Lin et al. (2004), obtained by fixing  $\alpha = -1.1$ ; M99 = Marinoni et al. (1999); N02 = Norberg et al. (2002); Co01 = Cole et al. (2001). The value of  $M_*$  of DP03 and N02 is corrected for the conversion from  $b_J$  to Johnson B, by making use of  $b_J - B = -0.28$  (B–V) (Blair & Gilmore 1982) and  $(B-V) \simeq 0.94$  (Norberg et al. 2002).

several authors, in different photometric bands (e.g., Balogh et al. 2001; Yagi et al. 2002; De Propris et al. 2003), even if a general consensus still lacks (Lobo et al. 1997; Trentham 1998; Phillipps et al. 1998; Beijersbergen et al. 2002; Mobasher et al. 2003; Chrislein & Zabludoff 2003; Lin et al. 2004) and conclusions also depend on the considered range of magnitudes.

The model predicts that while the most luminous “red” galaxies reside in clusters cores, the brightest “blue” galaxies ( $M_B < -22$ ) populate the field, but are not seen in clusters (compare panel a and c of Figure 3). This latter finding is in agreement with the observations of Trentham (1998), but in contrast with De Propris et al. (2003); in both cases, however, observational evidences are not very strong. De Propris et al. also report on an excess of very bright “blue” galaxies in cluster cores with respect to the envelopes, which we do not detect in our simulations. This might be an effect of the too rough way we assign positions to galaxies within DM haloes (see Section 3.2), and not a real problem of how galaxy formation is modelled, and we plan to investigate this issue in more detail later.

In agreement with the observations (Balogh et al. 2001; Yagi et al. 2002; De Propris et al. 2003), we find that *the LF of early-type galaxies has a flatter faint-end slope and a brighter characteristic magnitude, with respect to that of spirals, both in clusters and in the field.* This can be seen in Figure 5 for cluster environment and the K band, with model results for early and late type galaxies compared to the best-fit Schechter functions for non-emission-line and emission-line galaxies, as determined by Balogh et al. (2001) on the basis of the measured equivalent width of the [O II] emission line. We emphasize that the normalisation is *not* arbitrary in Figure

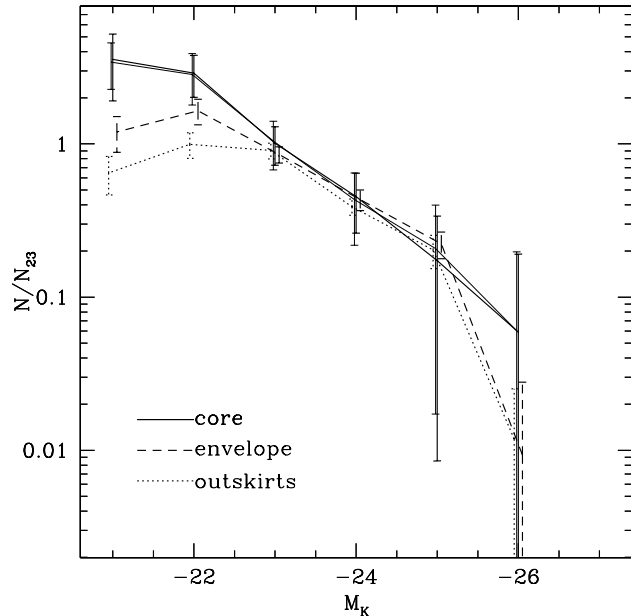


**Figure 4.** Dependence of the K band LF on environment. Curves and error bars represent the average LFs of the 15 simulations, and their rms dispersion about the mean, for three types of environment: cluster cores (thick solid line), cluster envelopes (dashed line), cluster outskirts (dotted line). The thin solid line traces the average LF for cluster cores when ram pressure stripping is neglected. Analogous trends are found in the B band. LFs are normalised to the number of galaxies with  $M_K \leq -23$ .

5: both model and observed LFs are normalised to the *total* number of cluster galaxies with  $M_K \leq -21$ . A similar agreement is found with the data of De Propris et al. (2003) in the  $b_J$  band, for galaxies types split following their spectral properties (Madgwick et al. 2002). This should be interpreted as a non trivial success of the model, particularly if one considers that our definition of morphological types (based on the bulge-to-disc luminosity in the B band) does not exactly correspond to those adopted in the observational studies.

## 4.2 Morphological fractions

The dependence of the mix of morphological types on cluster mass for our simulations is studied in Figure 6, for galaxies brighter than  $M_B = -17$  and  $M_B = -19$ , and for morphologies modelled by the bulge-to-disk blue luminosity ratio (Sect. 3.1). The total number of galaxies brighter than these magnitude limits in each cluster is given in Table 1 (columns 8 and 9). From Figure 6 we conclude that *the fractions of different morphological types do not show any clear systematic dependence on cluster richness.* The only trend is for a larger fraction, on average, of bright ( $M_B < -19$ ) spiral galaxies in low-mass clusters, but the significance is marginal.

On the other hand, the dependence on the luminosity cut is stronger: with respect to the global population, the brighter subsample shows a higher fraction of ellipticals and a lower fraction of spirals, independent of cluster mass. This is particularly significant in high-density environments, as apparent from Figure 7, where the cores, envelopes and outskirts of the 15 simulated clusters are considered separately: outside of clusters, the percentage of different morphological types is fairly independent of the considered cut in

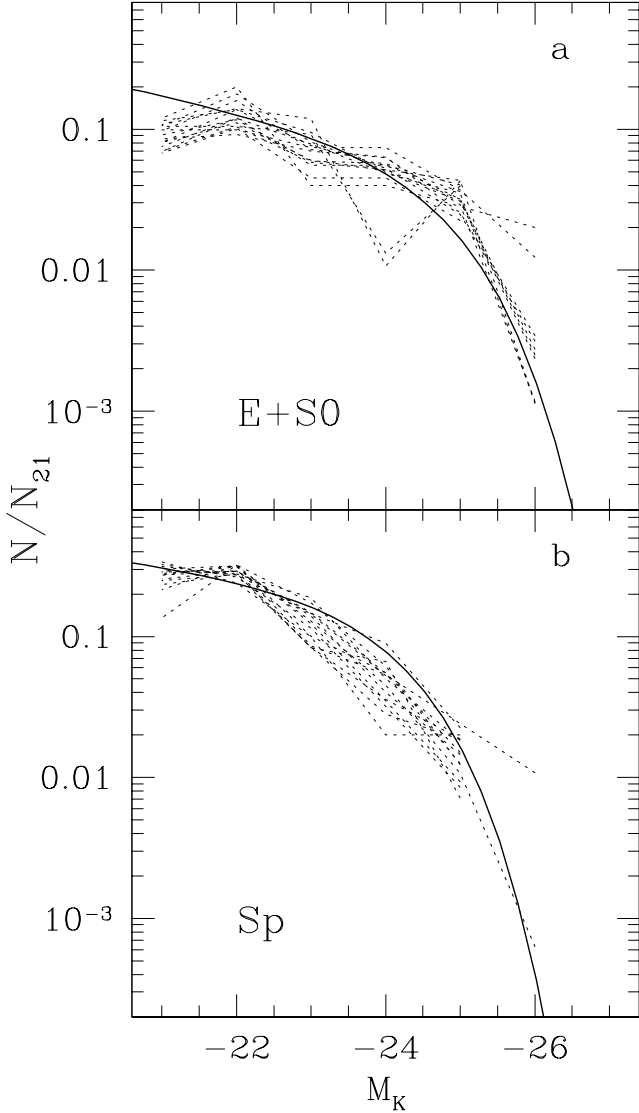


**Figure 5.** Dependence of the cluster K band LF on morphological types. Dotted lines show the 15 individual LFs for model ellipticals and lenticulars (*panel a*), and for model spirals (*panel b*), normalised to the total number of cluster galaxies with  $M_K \leq -21$ . Solid lines are the observed best-fit Schechter functions, with the same normalisation, as determined by Balogh et al. (2001) for non-emission-line and emission-line galaxies, respectively.

absolute magnitude, whereas changes in the luminosity selection limit lead to increasingly different morphological mixes when one moves towards the cluster cores. In other words, *the relative morphological mix in the inner regions shows larger variations from cluster to cluster and strongly depends on the magnitude limit, with spiral galaxies dominating for  $M_B < -17$ , and ellipticals and S0s catching up at  $M_B < -19$* . In comparison, *in the outskirts of clusters, the prevalence of spirals is overwhelming for any luminosity cut with the percentage of early-type galaxies never in excess of 20%*. In the intermediate density environment of cluster envelopes, late-type galaxies tend to dominate the overall population, even if their median fraction systematically decreases for increasing luminosity cut.

Our spiral fraction in cluster outskirts appears too high, in

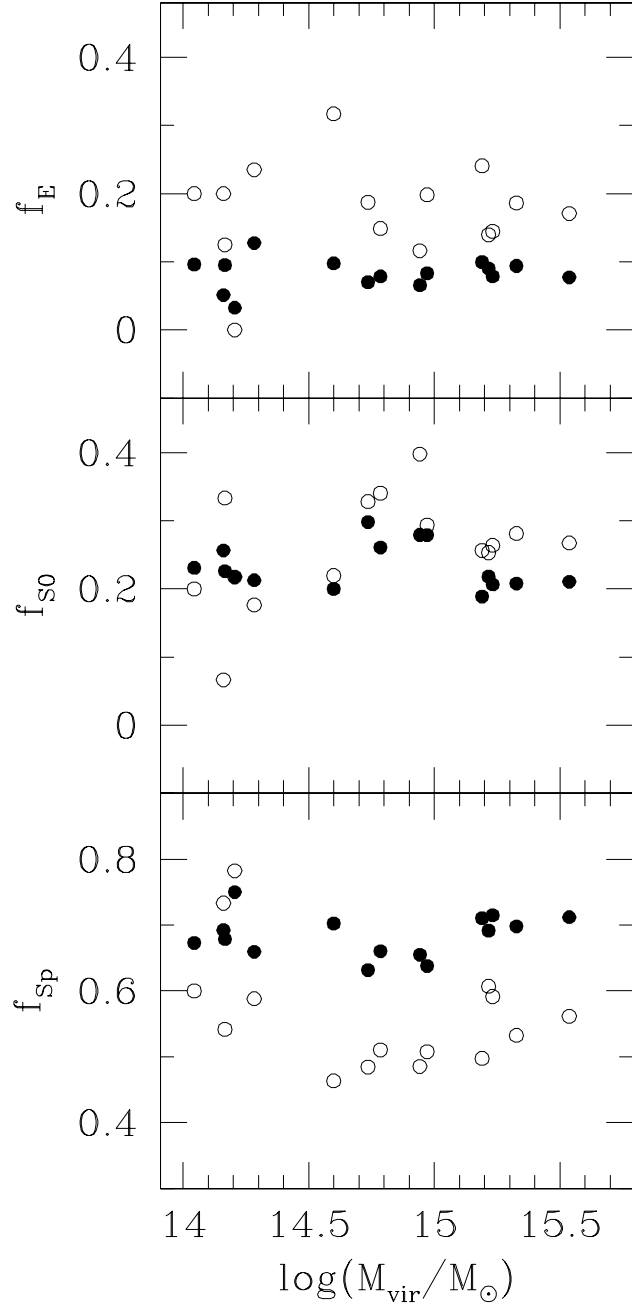


**Figure 6.** Dependence of galaxy morphological fractions on cluster mass. From top to bottom, the 3 panels show the fraction of ellipticals, lenticulars and spirals, as a function of the host DM halo virial mass. All galaxies within  $r_{vir}$ , having  $M_B < -17$  (solid circles) and  $M_B < -19$  (empty circles) are considered.

comparison to the morphological mix derived from the Stromlo-APM redshift survey (Loveday et al. 1996), for galaxies brighter than  $M_B = -18.8$  (E:S0:Sp = 13:11:76, see GALICS I). However, such a disagreement is most probably not due to the model itself, but rather to the different kind of environment considered in the present paper (the immediate outskirts of galaxy clusters), and in the Stromlo-APM redshift survey (the average field, which also includes clusters and super-clusters, where the early-type fraction is

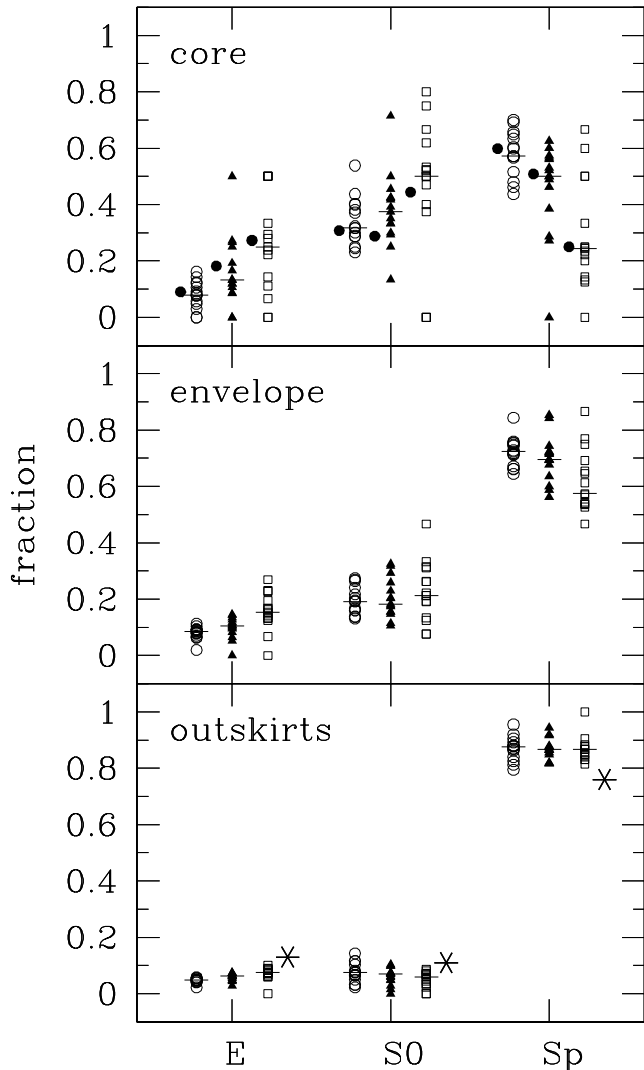


**Figure 7.** Dependence of galaxy morphological fractions on environment. The fractions of ellipticals, S0s and spirals are shown for three kinds of environment and for three magnitude selection limits. *From top to bottom:* cluster cores, envelopes, and outskirts. Empty circles are for galaxies brighter than  $M_B = -17$ , solid triangles for  $M_B < -18$ , and empty squares for  $M_B < -19$ . The short horizontal lines mark the medians of the distributions. Solid dots in the upper panel show the median values obtained if ram pressure stripping is not taken into account. Asterisks in the bottom panel mark the average morphological fractions in the field derived from the Stromlo-APM redshift survey, for galaxies brighter than  $M_B = -18.8$  (E:S0:Sp = 13:11:76).

higher). In fact, the Stromlo-APM mix is better reproduced by our model when applied to large scale cosmological simulations, where both high and low-density environments are represented (see GALICS I).

Moreover, *the comparison with observations in clusters is very satisfactory*, as apparent from Figure 8. The data are from Vogt et al. (2004), for all galaxies with measured position and redshift, and within a distance of  $2 \text{ Mpc}/h$  from the centres of a set of local clusters. According to the authors, the sample “starts to become significantly incomplete at B band magnitudes ranging from  $-18.5$  to  $-19.5$ ”. For a consistent comparison, we have therefore selected in

our 15 simulations all galaxies with the same distance from cluster centres and with  $M_B < -18.8$ . The left panel of Figure 8 indicates that the distribution of morphological mixes found in the simulations is in good agreement with that of the observed sample, with a large scatter from cluster to cluster, and similar median values. The right panel of Figure 8 shows that model results also reproduce the observed anti-correlation between the global fraction of spirals and that of lenticulars, with the global fraction of ellipticals staying almost constant around 15%. Note that a radial distance  $2 \text{ Mpc}/h$  is larger than the DM halo virial radius for 10 of our 15 clusters, and it corresponds to at least  $0.7 \times r_{\text{vir}}$  for the 5 most massive ones. In Figure 8, we are therefore considering the overall cluster population (brighter than  $M_B = -18.8$ ), not only the most central one, which explains why the spiral fraction is comparable to or larger than that of early-type galaxies.

### 4.3 Galaxy colours

It is well established that galaxy colours show a dependence on morphological type, as well as on environment, with ellipticals and S0s being redder and with tighter colour distributions than spirals, and with field galaxies being, on average, bluer than their cluster counterparts.

As a preliminary remark, *the colours of our simulated galaxies do not appear to systematically depend on cluster richness*: the colour distributions, both for early and late type galaxies, show approximately the same shape in all clusters, independently of the mass of the host DM halo. This statement holds for any colour and for any magnitude limit, as well as for galaxies populating the cluster as a whole, or simply the cores. Therefore, in the following, we will only focus on the *mean* colour distributions, obtained by averaging over the entire 15 cluster sample.

We study the dependence of galaxy colour on environment in Figure 9, where the B–V distributions in cluster cores are compared to those in the envelopes and in the outskirts, for early-type and late-type galaxies, separately. For both morphological types, *colours appear to be extremely homogeneous in cluster cores, whereas a tail of bluer galaxies develops when moving to regions of progressively lower density*. For ellipticals and S0s, the peak of the distribution stays around  $B-V \simeq 0.9$ , and the scatter about it remains quite small in all environments. The colour distribution of spirals, instead, changes completely, from strongly peaked around  $B-V = 0.9$  in cluster cores, to very dispersed around colours more than  $0.45 \text{ mag}$  bluer, in the outskirts. These trends do not change if we restrict the analysis to sub-samples of brighter galaxies, or if we consider other colours, and are in qualitative agreement with the observations.

A more quantitative study of the dependence of colours on morphological types is provided in Figure 10, where we directly compare the B–V and the V–K colour distributions of cluster ellipticals and S0s (dashed histograms), to those of spirals (empty histograms). For both colours, *spirals appear to be systematically bluer than early-type galaxies*. In B–V (panel a), the vast majority of early-type galaxies is well characterised by a single colour ( $B-V \simeq 0.9$ ) with a small ( $0.1 \text{ mag}$ ) dispersion, while spirals redder than  $B-V = 0.9$  are not found, and their distribution is wider (more dispersed) and shifted towards bluer colours. In V–K, the distributions are more dispersed and skewed towards red and blue colors for early and late type galaxies, respectively (panel b). Observational results are shown in the inserts of Figure 10, where data are taken from the *Galaxy On Line Database Milano Network* (hereafter GOLDMine, Gavazzi et al. 2003), which we corrected for

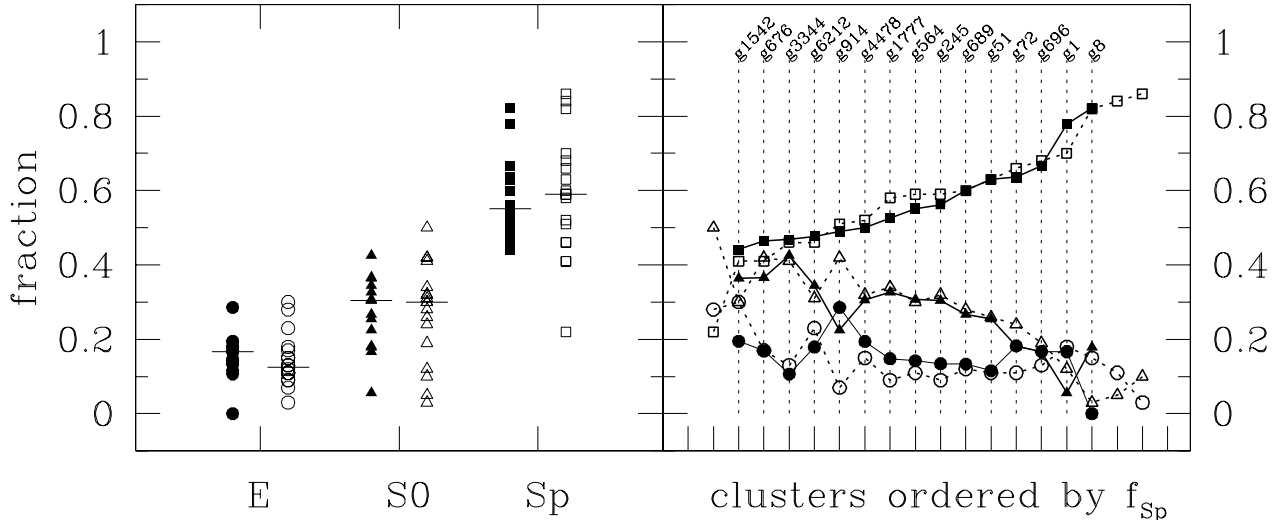


**Figure 8.** Comparison of the model morphological fractions to observations. Model galaxies have been selected with  $M_B < -18.8$  and within 2 Mpc/h from cluster centres, similarly to the observations of Vogt et al. (2004). *Left panel:* model results (solid symbols) are compared to observational data (empty symbols) from Table 1 of Vogt et al. (2004). The short horizontal lines mark the medians of the distributions. *Right panel:* distribution of the relative morphological fractions (represented with squares, triangles, and circles for spirals, lenticulars, and ellipticals, respectively) for clusters ordered by increasing spiral fraction, in the model (solid symbols), and in the observations (empty symbols); clusters are sorted out along the x-axis by increasing spiral fraction, with arbitrary spacing.

galactic extinction, as estimated by Schlegel et al. (1998), using the NASA/IPAC Extragalactic Database (NED), and k-corrected following Poggianti (1997). For the B–V colours we also show data from Prugniel & Simien (1996), which were already extinction and k-corrected. The general trends found for our model results are in qualitative agreement with the observations. More in detail, *the V–K distribution of simulated spirals well corresponds to the observed one, while their B–V colours are not blue enough and present and unobserved peak around  $B-V \simeq 0.9$ .* This is a drawback of the model, possibly due to the fact that gas accretion is not allowed on satellite galaxies in any DM halo, so that fewer new stars can form as redshift decreases, thus leading to older and redder stellar populations than the observed ones. *In B–V, a much better agreement is found for ellipticals and S0s, with the right colour for the peak of the distribution, and only a relatively small deficiency of slightly bluer ( $B-V \simeq 0.8$ ) and slightly redder ( $B-V \simeq 1$ ) galaxies.* However, *in V–K the whole colour distribution of ellipticals and S0s is 0.2 mag too red with respect to the observations.*

The model predictions for early-type galaxies are further compared to observations in Figure 11, in terms of the colour-magnitude relations (data are as in Figure 10, plus those from Bower, Lucey & Ellis 1992 in V–K. To the latter, which are already extinction corrected, we applied Poggianti’s k-corrections). Simulated galaxies do follow tight and well defined relations, especially for the B–V colour. In this case, both the slope and the scatter in model results reproduce well the observed ones. The V–K colour-magnitude relation less accurately matches the observations, showing an average shift of  $\sim 0.2$  mag, a too large scatter (too skewed towards red colours), and a flatter slope. As already discussed in Section 4.1, a discrepancy also exists in terms of a lack in the model of the brightest cluster galaxies ( $M_B \lesssim -22$  and  $M_V \lesssim -22.5$ ) found in the observations.

Note however that the exact shape of the colour distribution

depends quite sensitively on the definition of morphological types, which is not exactly the same in the model and the observations. Moreover, the way colours have been obtained (from the galaxy total light, as in the model, or within smaller central regions due to fixed aperture observations, for instance), as well as the adopted extinction and k-corrections, can easily lead to discordant results and therefore make it difficult to compare observations and models (see e.g. Kaviraj et al. 2004).

#### 4.4 Effects of ram pressure stripping

We find that *by including or neglecting ram pressure stripping in the model, galaxy properties only show mild variations.* The LFs obtained by taking into account or by “switching off” this process are almost indistinguishable. This is shown, for instance, in Figure 4 for cluster core environment, where the stripping should be maximally efficient. Also the effects on galaxy color distributions are completely negligible, as can be seen in Figure 9. The morphological mix in cluster cores appears to be mildly affected by ram pressure stripping, with a slight increase of the fraction of ellipticals and spirals, in spite of that of lenticulars, if the process is neglected (panel a in Figure 7). However, the effect is small and no systematic trends with cluster richness are found. The cold gas content of spiral galaxies is effectively smaller in clusters than in the outskirts, but this is mainly due to the different gas accretion, gas consumption, and star formation histories in the two kinds of environment: in dense environments, objects form earlier on average and therefore have shorter dynamical and star formation timescales. Moreover, field spirals in the model typically correspond to the central galaxy of the embedding DM haloes, and thus they can continuously accrete new cold gas onto their disks; cluster spirals, instead, are satellite galaxies, which can only consume their gas reservoir until its complete exhaustion. Thus, by the time the ram pressure

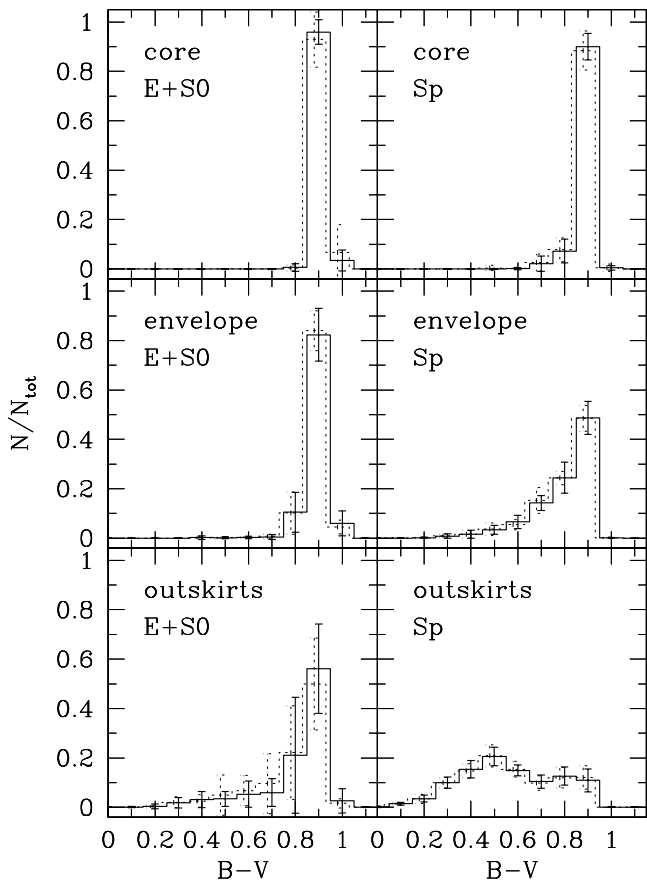


**Figure 9.** Dependence of galaxy B–V colours on environment. Average B–V colour distributions and rms dispersion about the mean, for early-type galaxies (*left panels*) and spirals (*right panels*), in three types of environment: cluster cores (*top panels*), envelopes (*middle panels*) and outskirts (*bottom panels*). Dotted histograms show the results if ram pressure stripping is not taken into account.

stripping process becomes efficient (cluster assembly epoch), most of the gas has already been processed in a large fraction of the cluster member galaxies, and similar results are found whether or not we include ram pressure in the model. We therefore confirm the conclusions of Okamoto & Nagashima (2003) that ram pressure stripping plays a minor role in galaxy transformations, provided a more accurate description of this process does not prove it to be more efficient by, say, an order of magnitude than our estimates.

## 5 SUMMARY AND DISCUSSION

In this paper, we have studied galaxy formation and evolution in clusters and in their outskirts, within the framework of the hierarchical merging scenario, by means of high-resolution re-simulations of massive DM haloes, and the GalICS hybrid galaxy formation model.

Numerical N-body simulations and a good mass resolution are both necessary to accurately follow the formation history of DM haloes, where observable galaxies form and evolve. An effective method, in terms of computational cost, consists in re-simulating with a larger number of particles a given halo or a given region selected from an already-run N-body simulation, thus increasing its mass resolution. In the present work, we have applied such a

technique to a sample of 15 massive DM haloes, increasing their mass resolution by a factor  $\sim 33$  or  $66$ , so that the evolution of all DM haloes of at least  $2$  or  $1 \times 10^{10} M_{\odot}/h$  can now be followed.

To detect haloes, construct their merging histories, and form galaxies within them, we have employed the GalICS model, that has been presented and tested against several observations of the local and high redshift Universe in the first and third papers of this series (Hatton et al. 2003; Blaizot et al. 2004). Here, GalICS is used to investigate whether (and how) galaxy properties depend on cluster richness (with our halo masses in the range between  $10^{14}$  and  $10^{15} M_{\odot}$ ), and on the density of the local environment (cluster cores, envelopes and outskirts). With respect to GALICS I, the improved mass resolution of our simulations have raised the necessity for a better description of the reionisation history of the Universe, needed to avoid an unobserved excess of galaxies at the faint-end of the LF. A semi-analytic description of ram pressure stripping has also been included, since this process is commonly considered to be important in cluster environment. Luminosity functions, morphological fractions and colours have been studied for all galaxies brighter than the magnitude limits imposed by our mass resolution:  $M_B = -16.75$ ,  $M_V = -17.5$ ,  $M_K = -20.5$ , in B, V and K bands, respectively. We now proceed to summarise and discuss our main results.

### 5.1 Luminosity function

- (i) The cluster LF appears to be universal, in all photometric bands: its shape varies from cluster to cluster, but it does not show any clear dependence on cluster richness (mass), at least in the galaxy luminosity and cluster mass ranges probed by the model.
- (ii) A gradual steepening of the faint-end of the LF with increasing density of the local environment (i.e., from cluster outskirts, to cluster envelopes, to the cores) is detected in all bands.
- (iii) In K, the brightest galaxies have similar luminosities both in cluster cores and in the outskirts, while in B, cluster central galaxies never attain the same high luminosities as their outskirts counterparts.
- (iv) The LF of cluster early-type galaxies is flatter than that of spirals.
- (v) A good agreement is found with respect to the observed cluster LFs, both in B and in K, and also for different morphological types considered separately. The main discrepancy consists in too faint luminosities of the brightest cluster members: galaxies brighter than  $M_B \simeq -22$  and  $M_K \simeq -26$  are absent in the model, but are found in the observations.
- (vi) The agreement is still satisfactory between the model LFs for the cluster outskirts and the observed LFs for the average field in the K band. In B, instead, the model predicts a too bright  $M_*$ , and a too flat faint-end slope, compared to the observed values.

Some notes of caution should be spent about the comparison between simulations and observations. For what concerns the model LF, its faint-end is very sensitive to the magnitude resolution limits and to the detailed modelling of reionisation squelching at high redshift, a process that is still poorly known and that also depends, in turn, on the mass resolution of the DM simulations (see Section 3.2). The bright-end, instead, is affected by galaxy merging, with both the frequency of this process and the exact characteristics of the merger end-products being modelled in a very approximated way. Finally, the exact values of the Schechter best fit parameters are not very robust, since they depend on the considered binning and range of magnitudes. On the side of observations,

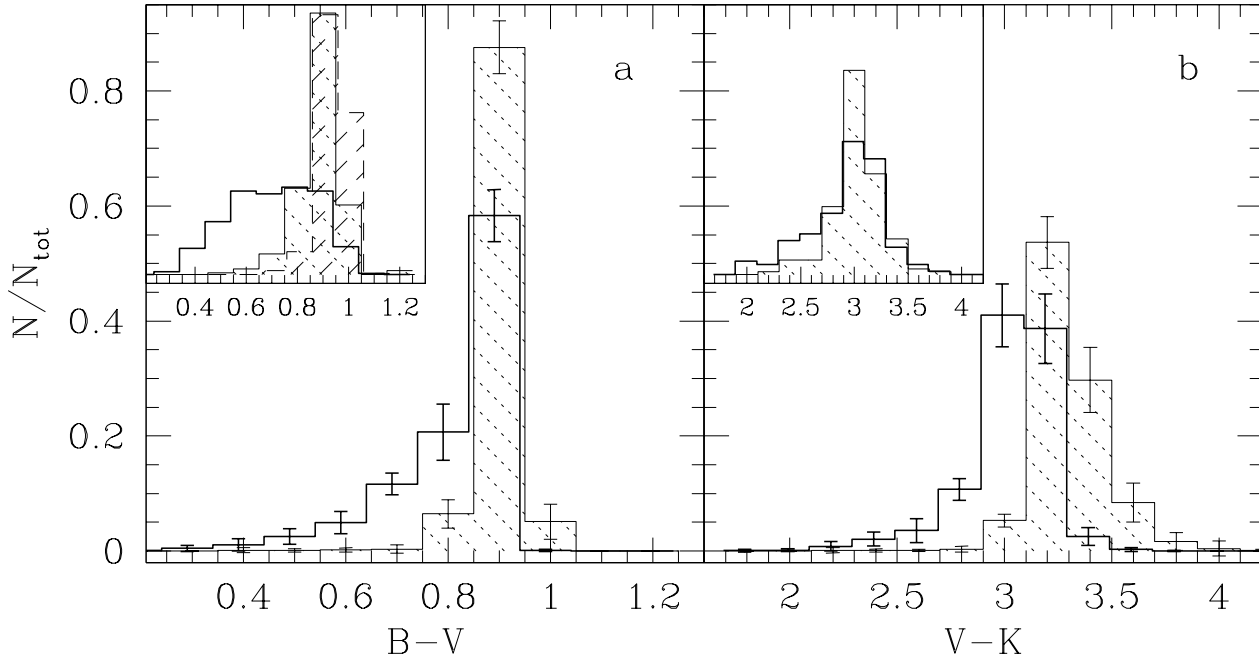


**Figure 10.** Dependence of galaxy B–V and V–K colours on morphological type. *Panel a:* average B–V colour distribution of cluster ellipticals and S0s (shaded histograms), compared to that of spirals (empty histogram). Only model galaxies within  $r_{\text{vir}}$  and with  $M_{\text{B}} < -17$  are considered. The analogous histograms in the insert (where values along the y-axis are arbitrary) refer to observed galaxies obtained from GOLDMine. The additional histogram in the left panel insert (shaded in long-dashed line) represents early-type galaxies from the Prugniel & Simien (1996) sample. *Panel b:* the same as in panel a, but for the V–K colour, and for galaxies brighter than  $M_{\text{V}} = -18.2$ . The insert shows the observed distribution obtained from GOLDMine. All observations are extinction and k-corrected (see text).

a general consensus on the exact shape of the LF, both in clusters and in the field, and on its dependence on the local density still lacks (see, e.g., Beijersbergen et al. 2002, Liske et al. 2003, Lin et al. 2004, and references therein). Results are quite sensitive to several factors, like the considered range of magnitudes, the inclusion/exclusion of the brightest cluster members, the adopted corrections (for incompleteness of the sample, surface brightness effects, etc.), and the method used for combining different samples and get the average LF. Also the way fits are performed can affect the results, with a single Schechter function often providing a poor description of the observed LFs (e.g., Popesso et al. 2004, and references therein). A further difficulty for a proper comparison between model and observations, as well as among different observational results, is added by the necessary transformation from one photometric band to another, that pass through uncertain and approximated average colour conversions.

We finally stress that our comparisons are mainly valid in terms of the overall shape of the LFs, while they do not provide information about the relative excess or deficiency of galaxies, since they depend on the adopted normalisation (as it is always the case when comparing functional shapes that are not identical): for instance, if we normalise our outskirts LF to the number of galaxies more luminous than  $M_{\text{B}} = -20.5$  (rather than  $M_{\text{B}} = -18.5$ ), we better recover the bright-end of the observed field LF, but further underestimate the fraction of faint objects. If one also considers that the types of environment, as well as the definitions of morphological types do not exactly correspond in the model and in the

observational studies, the agreements we find should be considered quite satisfactory.

## 5.2 Morphological fractions

- (i) No clear trend is found between the relative fractions of spirals, S0s and ellipticals and cluster richness in our results.
- (ii) The morphological mix shows quite a large scatter from cluster to cluster, and a significant dependence on the adopted magnitude cut, particularly in cluster cores. In fact, whereas for  $M_{\text{B}} < -17$  spirals are more abundant than ellipticals in the cores of all clusters, early-type galaxies dominate in most of the cases for  $M_{\text{B}} < -19$ .
- (iii) The morphological mix clearly changes with environment, from massively spiral-dominated in the outskirts, to a more balanced mix between spirals and ellipticals/S0s when moving to cluster cores.
- (iv) A good agreement with the observations is found for the morphological mix in clusters.
- (v) With respect to the observational data for the “average field”, we find an excess of spirals (and a deficiency of early-type galaxies) in our cluster outskirts.

While this latter discrepancy is probably related to the different kind of environment considered in the model and in the observations, the success at reproducing the cluster morphological mix is not trivial, particularly if one considers that different definitions of morphological types are adopted. Since galaxy positioning in the model is currently described in a rough way, we do not push the

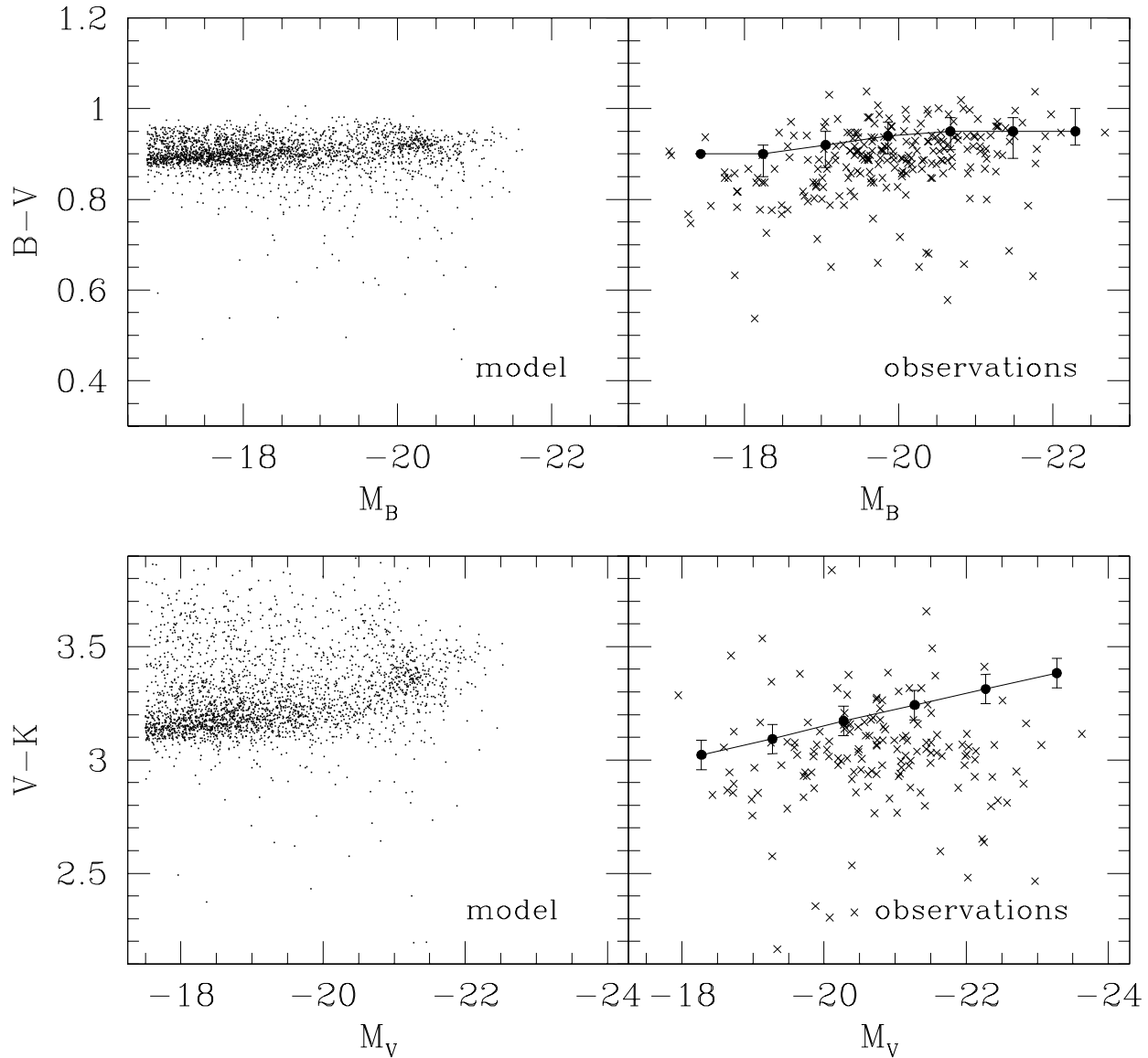


**Figure 11.** Colour-magnitude relations for cluster early-type galaxies. Model results are shown in the *left-hand panels*, observations (extinction and k-corrected) in the *right-hand panels*. *Upper panels:* B–V colour as a function of the B absolute magnitude. Model results are shown for all early-type galaxies within the virial radius of the 15 simulated clusters. Observational data extracted from the GOLDMine data base are shown as crosses, while the median colour-magnitude relation, with rms dispersion error bars, obtained from the data of Prugniel & Simien (1996) is plotted as a solid line. *Lower panels:* the same as in the upper panels, but for the V–K colour as a function of the V magnitude. Observations refer to the GOLDMine data (crosses), and to the mean colour-magnitude relation, with standard deviation error bars, for early-type galaxies in Coma cluster, from Bower et al. (1992; solid line).

comparison further and try to reproduce the observed cluster population gradients in more details, but we postpone this issue to a forthcoming paper.

### 5.3 Colour distributions

- (i) Galaxy colour distributions do not appear to depend on cluster richness, whatever our adopted magnitude limits, or whatever subsamples of galaxies we select in different environments.
- (ii) Early-type galaxies are systematically redder than spirals in all environments.

- (iii) Colours are very uniform in cluster cores, with a well defined peak around  $B-V=0.9$ , both for early and late type galaxies.

- (iv) The distributions become increasingly dispersed towards bluer colours when moving to environment of lower densities, still maintaining a peak at  $B-V \simeq 0.9$  in the case of the ellipticals and S0s, while completely changing to a flat and bluer distribution for spirals in cluster outskirts.

- (v) Compared to observational data from a sample of local clusters, the B–V colours of simulated spirals appear to be too uniform and too red, while a better agreement is found for the V–K.

- (vi) The B–V colour distribution and colour–magnitude relation of

early-type galaxies in clusters is in fairly good agreement with the observed ones, whereas a too flat slope, an average shift of  $\sim 0.2$  mag, and too large dispersion towards the red is found for the V–K colours.

The observed general trends of galaxy colours with morphological type (redder for early-type galaxies) and environment (redder and more uniform in denser environments) are thus reproduced by our simulations, but some discrepancies are also apparent. Disagreements are in the sense of not-blue-enough or too-red colours, and might be due to an imprecise dust modelling, as well as to the fact that gas accretion, and the consequent formation of new stars, is not allowed on non-central galaxies. Moreover, different factors contribute to make difficult an appropriate comparison between observations and model results: not only the already discussed differences in the adopted definitions of morphological types and environments, but also the way colours have been obtained and, in certain cases, corrected. In fact, the known internal colour gradients in galaxies, imply that data obtained from the galactic total light (as in our simulations), or from the luminosity integrated on smaller, central areas (possibly corrected afterwards for aperture effects) may substantially differ and bring to discordant colour–magnitude relations (e.g., Bender, Burstein & Faber 1993; Fioc & Rocca-Volmerange 1999; Scodreggio 2001; Kaviraj et al. 2004). When feasible, we have tried here to homogenize the model and observational results as much as possible, but part of the discrepancies might still be ascribable to aperture effects and errors in extinction and k-corrections.

#### 5.4 Ram pressure stripping

By means of a simplified formula, we have modelled the ram pressure stripping of cold gas from galactic discs, during the motion of galaxies through the diffuse hot intra-cluster medium. All results appear to be practically unaffected by the inclusion of this process in the model, in agreement with the conclusions of Okamoto & Nagashima (2003). We stress, however, that a more accurate modelling of this process is required before completely assessing its role in modifying galaxy properties during their cosmic evolution.

#### 5.5 Conclusions

The present paper is part of the series investigating the ability of the GalICS model to reproduce and predict a full set of observational data, in several photometric bands and environments, and at various redshifts. Here we have focussed on clusters of galaxies of different richnesses, at  $z = 0$ . A general good agreement between observations and theoretical results is found, even if some drawbacks are also apparent in the model. The main problems consist in a too faint luminosity of the brightest cluster galaxies, and a not yet satisfactory reproduction of galaxy colours, which tend to be too red (or not blue enough). While the present analysis concerns a limited set of galaxy properties in local clusters, we plan to extend it to other observables and to higher redshifts, thus addressing important issues, like, for instance, the Butcher–Oemler effect (Butcher & Oemler 1984), and the origin and time evolution of galaxy scaling relations, all of which should further constrain the model. Moreover, some improvement to GalICS is also planned, and is expected to help to better reproduce the observations. In particular, we intend to describe galaxy positioning and interaction rates within DM haloes in a more accurate way, i.e., by directly following sub-structures in the DM N-body simulations and associating the baryonic galaxies

to them. This is expected to have several and relevant effects on final results (e.g., Springel et al. 2001b), since many galaxy properties (like the morphology, the stellar content, the overall luminosity and the dynamical characteristics) depend more or less strongly on the merging history of the galaxy. Allowing gas cooling on satellite (non central) galaxies, taking into account other sources of feedback, like type Ia supernovae, and following the growth of central super massive black holes and their effects on galaxy properties should also help to describe galaxy formation in a more suitable way. Then, all the analysis in the papers of this series, already published and in preparation, will finally give a complete judgement of the ability of the GalICS model, and, in turn, of the hierarchical merging scenario, to describe how galaxies form and evolve in the Universe.

#### ACKNOWLEDGMENTS

B.L. thanks Jeremy Blaizot, Lucia Pozzetti, Gianni Zamorani, Luca Ciotti and Simon White for many useful discussions. B.L. is also in debt with Volker Springel, Bepi Tormen, and Naoki Yoshida for their help with the N-body simulations. We acknowledge the anonymous referee for useful comments. Simulations have been run with GADGET (Springel et al. 2001a) on the IBM SP2 of the CINES (Montpellier, France), and the CRAY T3E of the RZG Computing Center (Munich, Germany). This research has made use of the GOLDMine Database (Gavazzi et al. 2003), and the NASA/IPAC Extragalactic Database (NED) which is operated by the Jet Propulsion Laboratory, California Institute of Technology, under contract with the National Aeronautics and Space Administration. B.L. is supported by a post-doc fellowship by Italian INAF.

#### REFERENCES

- Abadi, M.G., Moore, B., & Bower, R.G., 1999, MNRAS 308, 947  
 Balogh, M.L., Christlein, D., Zabludoff, A.I., & Zaritsky, D., 2001, ApJ 557, 117  
 Beijersbergen, M., Hoekstra, H., van Dokkum, P.G., van der Hulst, T., 2002, MNRAS 329, 385  
 Bender, R., Burstein, D., & Faber, S.M. 1993, ApJ 411, 153  
 Biermann, P., & Shapiro, S.L., 1979, ApJ 230L, 33  
 Blair, M. & Gilmore, G., 1982, PASP, 94, 741  
 Blaizot, J., Guiderdoni, B., Devriendt, J.E.G., Bouchet, F.R., Hatton, S.J., & Stoehr, F., 2004, MNRAS 352, 57 (GALICS III)  
 Blanchard, A., Valls-Gabaud, D., & Mamon, G. A., 1992, A&A 264, 365  
 Bower, R.G., Lucey, J.R., & Ellis, R.S., 1992, MNRAS 254, 601  
 Butcher, H., & Oemler, A.Jr., 1984, ApJ, 285, 426  
 Chamaroux, P., Balkowski, C., & Gérard, E., 1980, A&A 83, 38  
 Christlein D., & Zabludoff A., 2003, ApJ 591, 764  
 Cole, S., Aragon-Salamanca, A., Frenk, C.S., Navarro, J.F., Zepf, S.E., 1994, MNRAS 271, 781  
 Cole, S., Lacey, C.G., Baugh, C.M., & Frenk, C.S., 2000, MNRAS 319, 168  
 Cole, S., et al., 2001, MNRAS 326, 255  
 Davis, M., Efstathiou, G., Frenk, C.S., & White, S.D.M., 1985, ApJ 292, 371  
 De Lucia, G., Kauffmann, G., Springel, V., White, S.D.M., Lanzoni, B., Stoehr, F., Tormen, G., & Yoshida, N., 2004a, MNRAS 348, 333  
 De Lucia, G., Kauffmann, G., & White, S.D.M., 2004b, MNRAS 349, 1101  
 De Propriis R., et al., 2003, MNRAS 342, 725  
 Devriendt, J.E.G. Guiderdoni, B., & Sadat, R., 1999, A&A 350, 381  
 Diaferio, A., Kauffmann, G., Balogh, M.L., White, S.D.M., Schade, D., & Ellingson, E., 2001, MNRAS 323, 999  
 Dressler, A., 1980, ApJ 236, 351

- Dressler, A., Oemler, A.J., Couch, W.J., Smail, I., Ellis, R.S., Barger, A., Butcher, H., Poggianti, B.M., & Sharples, R.M., 1997, *ApJ* 490, 577
- Eke, V.R., Cole, S., & Frenk, C.S., 1996, *MNRAS* 282, 263
- Fioc, M., & Rocca-Volmerange, B., 1999, *A&A* 351, 869
- Gao L., White S.D.M., Jenkins A., Stoehr F., & Springel V., 2004, *MNRAS* 355, 819
- Gavazzi, G., Boselli, A., Donati, A., Franzetti, P., & Scodreggio, M., 2003, *A&A* 400, 451 (GOLDMine)
- Giovanelli, R., Chincarini, G.L., & Haynes, M.P., 1981, *ApJ* 247, 383
- Gunn, J.E., & Gott, J.R., 1972, *ApJ* 176, 1
- Hatton, S., Devriendt, J.E.G., Ninin, S., Bouchet, F.R., Guiderdoni, B., & Vibert, D., 2003, *MNRAS* 343, 75 (*GALICS* I)
- Helly, J.C., Cole, S., Frenk, C.S., Baugh, C.M., Benson, A., & Lacey, C., 2003, *MNRAS* 338, 903
- Kauffmann, G., Colberg, J.M., Diaferio, A., & White, S.D.M., 1999, *MNRAS* 303, 188
- Kauffmann, G., White, S.D.M., & Guiderdoni, B., 1993, *MNRAS* 264, 201
- Kaviraj, S., Devriendt, J.E.G., Ferreras, I., & Yi, S.K., 2004, *MNRAS* in press (astro-ph/0401126)
- Kenney, J.D.P., van Gorkom, J.H., & Vollmer, B., 2004, *AJ* 127, 3361
- Lacey, C., & Cole, S., 1994, *MNRAS* 271, 676
- Lanzoni, B., Cappi, A., & Ciotti, L., 2003, *MSAIS* 1, 145
- Lanzoni, B., Ciotti, L., Cappi, A., Tormen, G., & Zamorani, G., 2004, *ApJ* 600, 64
- Lin, Y., Mohr, J.J., & Stanford, S.A., 2004, *ApJ* 610, 745
- Liske, J., Lemon, D.J., Driver, S.P., Cross, N.J.G., & Couch, W.J., 2003, *MNRAS* 344, 307
- Lobo, C., Biviano, A., Durret, F., Gerbal, D., Le Fèvre, O., Mazure, A., & Slezak, E. 1997, *A&A* 317, 385
- Lopez-Cruz, O., Yee, H.K.C., Brown, J.P., Jones, C., & Forman, W., 1997, *ApJ* 475, 97
- Loveday J., Peterson B.A., Maddox S.J., & Efstathiou G., 1996, *ApJS* 107, 201
- Lumsden, S.L., Nichol, R.C., Collins, C.A., & Guzzo, L., 1992, *MNRAS* 258, 1
- Madgwick, D.S., et al., 2002, *MNRAS* 333, 133
- Mamon, G.A., 1992, *ApJ* 401, L3
- Mamon, G.A., 2000, in “Dynamics of Galaxies: from the Early Universe to the Present, 15th IAP meeting”, F. Combes, G.A. Mamon, & V. Charmandaris eds., ASP Conference Series, Vol. 197, p. 377 (astro-ph/9911333)
- Marinoni, C., Monaco, P., Giuricin, G., & Costantini, B., 1999, *ApJ* 521, 50
- Mathis, H., Lemson, G., Springel, V., Kauffmann, G., White, S.D.M., Eldar, A., & Dekel, A., 2002, *MNRAS* 333, 739
- Melnick, J., & Sargent, W.L.W., 1977, *ApJ* 215, 401
- Mobasher, B. Colless, M., Carter, D., Poggianti, B.M., Bridges, T.J. et al. 2003, *ApJ* 587, 605
- Moore, B., Lake, G., & Katz, 1998, *ApJ* 495, 139
- Norberg, P., Cole, S., Baugh, C.M., Frenk, C.S., Baldry, I. et al., 2002, *MNRAS* 336, 907
- Okamoto, T., & Nagashima, M., 2001, *ApJ* 547, 109
- Okamoto, T., & Nagashima, M., 2003, *ApJ* 587, 500
- Paolillo, M., Andreon, S., Longo, G., Puddu, E., Gal, R.R., Scaramella, R., Djorgovski, S.G., & de Carvalho, R., 2001, *A&A* 367, 59
- Phillipps, S., Driver, S.P., Couch, W.J., Smith, R. M. 1998, *ApJ* 498, L119
- Poggianti, B.M., 1997, *A&AS* 122, 399
- Popesso, P., Boehringer, H., Voges, W., 2004, *A&A* in press (astro-ph/0410011)
- Prugniel, P., & Simien, F., 1996, *A&A* 309, 749
- Roukema, B.F., Peterson, B.A., Quinn, P.J., & Rocca-Volmerange, B., 1997, *MNRAS* 292, 835
- Schechter, P., 1976, *ApJ* 203, 279
- Schlegel, D.J., Finkbeiner, D.P., & Davis, M., 1998, *ApJ* 500, 525
- Scodreggio, M., 2001, *AJ* 121, 2413
- Simien, F., & de Vaucouleurs, G., 1986, *ApJ* 302, 564
- Solanes, J.M., & Salvador-Solé, E., 1992, *ApJ* 395, 91
- Springel V., Yoshida N., & White S.D.M., 2001a, *New Astronomy*, 6, 79
- Springel, V., White, S.D.M., Tormen, G., & Kauffmann, G., 2001b, *MNRAS* 328, 726
- Somerville, R.S., & Primack, J.R., 1999, *MNRAS* 310, 1087
- Tormen G., Bouchet F., & White S.D.M., 1997, *MNRAS* 286, 865
- Trentham, N., 1998, *MNRAS* 294, 193
- Trentham, N. & Mobasher, B., 1998, *MNRAS* 299, 488
- Trentham, N., & Hodgkin, S., 2002, *MNRAS* 333, 423
- Tytler, D., Fan, X.-M., & Burles, S., 1996, *Nat*, 381, 207
- Valageas, P., & Silk, J., 1999, *A&A* 347, 1
- Valotto, C.A., Nicotra, M.A., Muriel, H., & Lambas, D.G., 1997, *ApJ* 479, 90
- Vogt, N.P., Haynes, M.P., Giovanelli, R., & Herter, T., 2004, *AJ* 127, 3300
- White, S.D.M., & Frenk, C.S., 1991, *ApJ* 379, 52
- Whitmore, B.C., Gilmore, D.M., & Jones, C., 1993, *ApJ* 407, 489
- Yagi M., Kashikawa N., Sekiguchi M., Doi M., Yasuda N., Shimasaku, K., & Okamura S., 2002, *AJ* 123, 66
- Yoshida N., Sheth R.K., & Diaferio A., 2001, *MNRAS* 328, 669

This paper has been typeset from a  $\text{\TeX}/\text{\LaTeX}$  file prepared by the author.